Aeroelastic Demonstrator Wing Design for Maneuver Load Alleviation Under Cruise Shape Constraint

Sodja, J.; Werter, N.P.M.; De Breuker, R.

DOI
10.2514/1.C035955

Publication date
2021

Document Version
Final published version

Published in
Journal of Aircraft: devoted to aeronautical science and technology

JOURNAL OF AIRCRAFT
Vol. 58, No. 3, May–June 2021

Aeroelastic Demonstrator Wing Design for Maneuver Load Alleviation Under Cruise Shape Constraint

Jurij Sodja,* Noud P. M. Werter,† and Roeland De Breuker‡
Delft University of Technology, 2629 HS Delft, The Netherlands

https://doi.org/10.2514/1.C035955

Application of the aeroelastic analysis and design framework developed at Delft University of Technology to a design of two aeroelastically tailored composite wings for a flying demonstrator is presented. The objective of the design process is to minimize structural mass of the wing while maintaining a target cruise shape. For this purpose, the jig shape of the wing is parameterized and becomes an integral part of the optimization, while the cruise shape is maintained by means of a constraint. Additionally strength, buckling, aeroelastic stability constraints, and a number of other design requirements have been introduced to obtain a feasible and flight-worthy design. Two wing types were designed: the reference wing and the tailored wing. The difference between the two wings is in the definition of the laminates comprising each wing. The reference wing was designed with symmetric-balanced laminates, while symmetric-unbalanced laminates were used for the tailored wing. The comparison is performed in terms of laminate stiffness and thickness distribution along the span, jig twist, and the aeroelastic response covering elastic deformations, aerodynamic load distribution, and wing root loads, showing a significant mass reduction for the tailored wing compared to the reference wing.

Nomenclature

$\hat{\boldsymbol{A}}$	=	membrane thickness-normalized laminate stiffness matrix, N/m^2
$\boldsymbol{C}$	=	Timoshenko cross-sectional stiffness matrix
C_{Lp}	=	roll coefficient due to rolling (roll damping), rad^{-1}
$C_{L\delta}$	=	roll coefficient due to control surface deflection, rad^{-1}
$\hat{\boldsymbol{D}}$	=	bending thickness-normalized laminate stiffness matrix, N/m^2
EI	=	bending stiffness, N · m^2
E_{11}^A	=	membrane modulus of elasticity, N/m^2
E_{11}^D	=	bending modulus of elasticity, N/m^2
e	=	shear center location with respect to beam reference axis, % chord
F_1, F_2, F_3	=	1, 2, 3 component of cross-sectional force, N
GJ	=	torsional stiffness, N · m^2
g	=	gravitational acceleration, m/s^2
K	=	bend–twist coupling, N · m^2
KDF	=	material knockdown factor
L	=	lift, N
M_x, M_y, M_z	=	x, y, z components of moment, N · m
M_1, M_2, M_3	=	1, 2, 3 components of cross-sectional moment, N · m
m	=	aircraft mass, kg
n	=	load factor
p	=	smoothing parameter
SF	=	safety factor, 1.5
$\boldsymbol{T}$	=	axes transformation matrix
V_x, V_y, V_z	=	x, y, z components of shear force, N
V1A, V2A, V3A, V4A	=	lamination parameters governing membrane stiffness
V1D, V2D, V3D, V4D	=	lamination parameters governing bending stiffness
v_∞	=	flight velocity, m/s
w_i	=	fitting weights
y	=	spanwise coordinate, m
ε	=	strain
η_{ail}	=	control effectiveness
θ	=	polar angle, deg
θ_{fit}	=	cubic spline for fitting jig twist, deg
θ_{jig}	=	jig twist, deg
κ	=	curvature, m^{-1}

Subscripts

x, y, z	=	along global x, y, z directions
1	=	aligned with beam axis
2, 3	=	normal to beam axis

Presented as Paper 2018-2153 at the 2018 AIAA/ASCE/AHS/ASC Structures, Structural Dynamics, and Materials Conference, Kissimmee, FL, January 8–12, 2018; received 3 April 2020; revision received 30 July 2020; accepted for publication 11 November 2020; published online 24 February 2021.

*Senior Researcher, Faculty of Aerospace Engineering, Kluyverweg 1; j.sodja@tudelft.nl. Member AIAA.
†Researcher, Faculty of Aerospace Engineering, Kluyverweg 1.
‡Associate Professor, Faculty of Aerospace Engineering, Kluyverweg 1; r.debreuker@tudelft.nl. Senior Member AIAA.

I. Introduction

AEROELASTIC design of composite wings has two significant aspects: aeroelastic optimization of the wing and optimization of the composite material comprising the structural members of the wing, often referred to as composite tailoring. Both aspects are tightly coupled by the interactions between aerodynamic loads and structural and material properties.

Over time, a sequential and an integrated approach to aeroelastic design have evolved. Interestingly, one of the earliest examples of aeroelastic optimization of aircraft wings, presented by Haftka in 1977 [1], used an integrated design approach to perform a tradeoff between minimum induced drag and minimum structural weight of the wing. In this Paper, composite materials are also considered to some extent, by varying the ratio between the 0, 90, and ±45 deg plies in the wing skins. Later, Grossman et al. [2] compared integrated and sequential aeroelastic optimization in the design of a sailplane wing. It was concluded that integrated design yielded superior performance due to better exploitation of interactions between aerodynamic loads and structural response. Nevertheless, the sequential design approach is still widely used today because the overall design problem can be split into smaller subproblems in which each subproblem can be optimized individually. Moreover, already existing results, such as an optimized cruise shape of the wing, can be reused if available. A recent example of such an approach is presented by Stodieck et al. [3], among others, in which

a predefined 1g shape of the wing is used as a constraint. The integrated aeroelastic design approach has evolved mainly into coupling high-fidelity computational fluid dynamics (CFD) and computational structural dynamics (CSD) models. The aerostructural adjoint method is commonly used for the calculation of sensitivities to enable gradient-based optimization of the global performance of an aircraft, such as range or fuel burn. The integrated design approach, however, comes at the cost of substantial implementation and computational effort. Recent examples of such work were presented by Kenway et al. [4], Brooks et al. [5], and Achard et al. [6], among others.

In the sequential design approach, aerodynamic efficiency is usually ensured by requiring the deformed shape of the wing to comply with the prescribed flight shape under the given flight conditions. The idea is that the cruise shape can be derived using high-fidelity CFD simulations or wind tunnel testing a priori, which should eliminate the accuracy limitations of the aerodynamic model used in the subsequent aeroelastic design. In practice, however, the aerodynamic model will still affect the fidelity of the result through the aerodynamic loads used to deform the jig shape into the prescribed flight shape. Two methods have been established to ensure that the flight shape constraint is met in the subsequent aeroelastic optimization. The first method often referred to as the inverse method formulates the aeroelastic problem directly on the deformed flight shape, and the jig shape is found in a subsequent step by reversing the exerted aerodynamic loads [1,7]. The advantage of this approach is that the jig shape does not require any specific parametrization and hence does not introduce additional design variables into the optimization problem. The inverse method has recently been used by Stanford et al. [8] and Stodieck et al. [3], among others. The second method includes the desired flight shape of the wing in the optimization problem as a constraint, and the jig shape is parameterized by a set of design variables which form part of the optimization problem. For example, Livne et al. [9,10] parameterized the jig shape as an out-of-plane deflection using a polynomial function of the spanwise and chordwise coordinate. Jig shape parametrization is also an essential part of the integrated design approach. In this context, the jig shape requires a much richer parameterization to also allow planform and span optimization of the wing. Brooks et al. [5] parameterized the jig shape of the wing using the free form deformation approach (FFD) [11] to control the span, spanwise twist, and planform of the wing.

The structural part of the optimization process does not need to be limited just to structural sizing. It can also include topological optimization of the structure. For example, optimal rib and spar distribution were investigated by Stanford et al. [12,13] while De et al. [14] and Zhao and Kapanta [15] investigated topology optimization using curvilinear spars and ribs.

Aeroelastic tailoring of composites has been researched extensively over the years. A summary of early research on aeroelastic tailoring of swept and unswept wings has been made by Shirk et al. [16]. More recently, Qin et al. [17,18] have researched the aeroelastic instability of composite, thin-walled beams to investigate the effect of aeroelastic tailoring. Several papers on the use of aeroelastic tailoring in general and its potential benefits have been written by Weisshaar [19], Danlin and Weisshaar [20], Livne and Weisshaar [21], and Weisshaar and Duke [22]. More specific research on the use of aeroelastic tailoring has been performed to minimize structural weight [23–28], to maximize flutter speed [25,26,29–32], to optimize the gust response characteristics of wings [33,34], and on the effect of tow-steered composites on wing aeroelastic characteristics [3,5]. An example of the use of aeroelastic tailoring in nonaerospace applications is the research by Thuwis et al. [35] of aeroelastic tailoring of the rear wing of an F1 car.

In addition to several numerical studies, experiments have been performed on tailored composite plates to assess the divergence and flutter characteristics of such structures [36–40]. These experiments have been performed on platelike structures; hence, they are unsuitable for validation of aeroelastic design frameworks dealing with wing structures having a closed-cell cross-section. Wind tunnel experiments involving such tailored composite wings with a closed-cell cross-section have been presented only recently by Werter et al. [41] and Sodja et al. [42].

Substantial theoretical and experimental research has been already performed. Nevertheless, experimental data obtained in a real-life environment, outside the laboratory, which can be used for the assessment of the benefits of aeroelastic tailoring for maneuver load alleviation and the validation of aeroelastic design frameworks, are still scarce. One of the goals of the Flutter Free FLight Envelope eXpansion for ecOnomical Performance improvement (FLEXOP) project,[§] funded by the European Union Horizon 2020 framework, is to demonstrate aeroelastic tailoring for manoeuvre load alleviation (MLA) in flight using an unmanned flying demonstrator and to assess the tailoring benefits. Therefore, two sets of wings, the reference and the tailored wing, are optimized with the same design requirements except for the general definition of the laminates used in each wing. Symmetric-balanced laminates are used in the reference wing, while symmetric-unbalanced laminates are used in the tailored wing. Therefore, the laminates comprising the reference wing cannot exhibit any extension–shear or bend–twist couplings, which are the primary mechanism for passive MLA as far as composite tailoring is concerned. Moreover, to obtain realistic estimates of MLA benefits due to the composite tailoring, a cruise shape constraint is enforced in the optimization process to limit excessive composite tailoring and to ensure that both wings have the same aerodynamic properties in cruise.

The objective of this Paper is to present and compare the optimized designs of the reference and tailored wing obtained using the analysis and design framework developed at Delft University of Technology. The Paper is organized as follows. First, the aeroelastic framework used to perform the design studies is briefly introduced in Sec. II. Introduction of the cruise shape as a design constraint is explained in Sec. III, followed by an explanation of the other design requirements in Sec. IV. Finally, the results obtained are discussed in Sec. V, followed by the conclusions in Sec. VI.

II. Aeroelastic Design Framework

An aeroelastic analysis and design framework was developed at the Delft University of Technology to optimize the structural design of aircraft wings at the conceptual design stage by including aeroelastic effects. A detailed explanation of the aeroelastic design framework is given by Werter and De Breuker [43] and Werter [44], while the validation of the framework against wind tunnel tests and reference cases accessible in the open literature has been presented in [41,43,44]. Therefore, only a brief overview of the framework is given here.

The aeroelastic analysis and optimization loop of the framework is depicted in Fig. 1. The loop starts with the definition of the wing geometry, material properties, and load cases as inputs. At this stage, the wing geometry is also partitioned into several design regions, each having its own laminate properties, which are defined using lamination parameters and laminate thickness, which results in a complete laminate definition by a fixed number of continuous design variables regardless of the laminate thickness, thereby allowing for the use of efficient, gradient-based optimizers.

In each iteration, the composite laminate properties used for the wing skins and spars are updated based on the prescribed material properties and the lamination parameters and thicknesses generated by the optimizer. The beam model is then generated by performing the cross-sectional analysis of the wing cross-section, accounting for the laminate properties. Thereby, the Timoshenko cross-sectional stiffness matrix with respect to the beam reference axis is generated for each beam element along the wing span. A detailed explanation of the cross-sectional analysis is given by Ferede and Abdalla [45].

Next, a geometrically nonlinear, static aeroelastic analysis for each load case is carried out. The static aeroelastic analysis closely couples a geometrically nonlinear Timoshenko beam model based on the

[§]FLEXOP Consortium, "Flutter Free Flight Envelope Expansion for Economical Performance Improvement," available online at https://flexop.eu [accessed 25 June 2020].

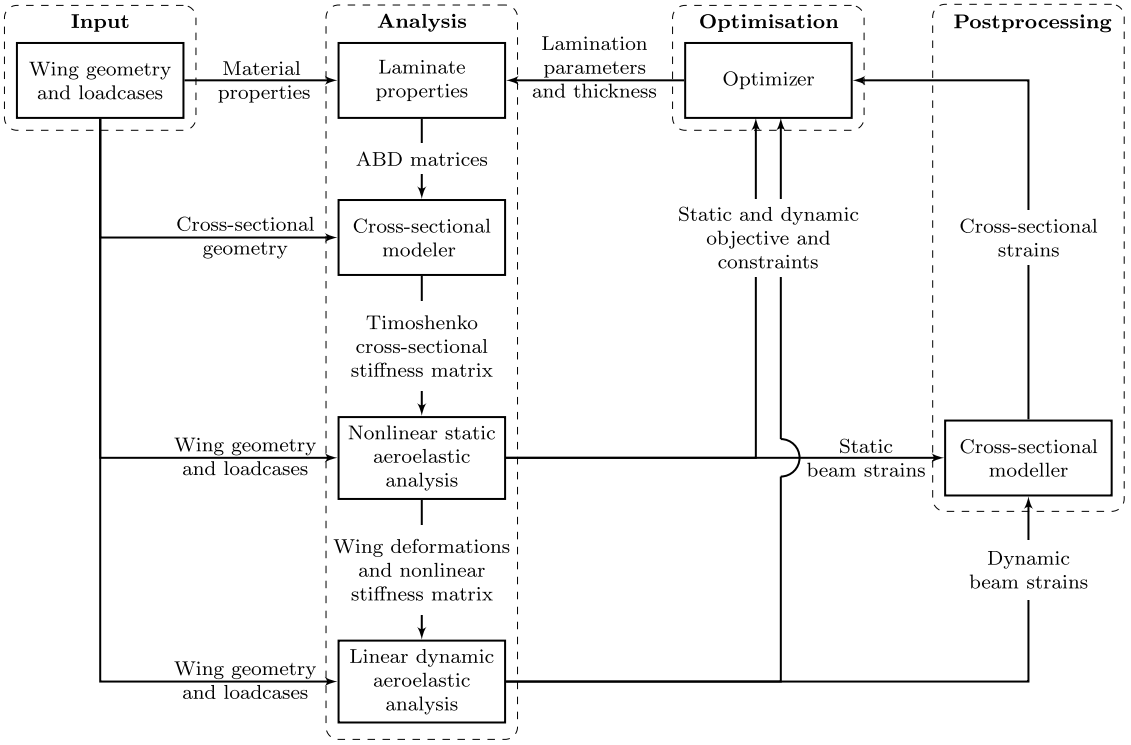

Fig. 1 Schematic representation of the aeroelastic analysis and optimization loop [43].

corotational formulation and a vortex lattice aerodynamic model. A geometrically nonlinear aeroelastic solution is obtained by using the load control and Newton–Raphson root finding method. A geometrically nonlinear model is used to account for large deformations due to applied loads and enforcement of the cruise shape constraint by morphing of the unloaded shape of the wing. The selected structural and aerodynamic models result in a computationally efficient model suitable for optimization.

To account for the effects of gravity due to structural and nonstructural masses and engine thrust, the model also includes eccentric follower and nonfollower forces based on the same corotational formulation already used for the structural model.

Dynamic phenomena, such as response to gust excitation and aeroelastic stability, are accounted for by linearization of the nonlinear aeroelastic model around its static equilibrium solution. Eigenvalue analysis of the linearized system matrix is used to evaluate aeroelastic stability constraints in the optimization problem.

In addition to aeroelastic stability constraints, control effectiveness is also evaluated to ensure sufficient control authority in the selected design load cases. Control effectiveness constraint is formulated as a negative ratio between the roll coefficient, $C_{L\delta}$, due to control surface deflection δ and the roll coefficient due to roll damping C_{Lp},

$$\eta_{\mathrm{ail}} = -C_{L\delta}/C_{\mathrm{Lp}} = (p_{\mathrm{roll}}s)/(\delta v_\infty) \tag{1}$$

where p_{roll} represents the steady roll rate for a given control surface deflection; s and V_∞ represent the wing semispan and the flight velocity. Aileron efficiency is evaluated by conducting antisymmetric aerodynamic analysis around steady symmetric aeroelastic equilibrium.

The strains in the three-dimensional wing structure are retrieved in a postprocessing step by using the cross-sectional modeler to convert beam strains and curvatures to skin strains. This allows for the evaluation of various structural constraints such as strength and buckling constraints.

The strength constraint is based on the implementation of the Tsai–Wu failure criterion as proposed by IJsselmuiden et al. [46] and Khani et al. [47], which guarantees a convex failure-free envelope in the lamination parameter space. The failure-free envelope is expressed as a contour of maximum allowable principal strains for which no failure should occur regardless of the retrieved ply orientations in the laminate. A strength reserve factor r_S is defined as the ratio between the norm of the observed strain and the norm of the maximum allowable strain. For the strength constraint not to be critical, r_S must satisfy

$$r_S < \mathrm{KDF}/\mathrm{SF} \tag{2}$$

where SF and KDF represent the safety factor and the total material knockdown factor.

The buckling constraint is evaluated for each buckling panel, which is defined as a patch of the laminate delimited by the ribs and spars. Each panel is approximated by a flat plate of constant stiffness with simply supported boundary conditions on all edges and subject to constant in-plane loading. The loading is retrieved using the cross-sectional modeler [44]. In a way similar to the strength reserve factor r_S, the inverse buckling reserve factor r_B is calculated as the ratio between the applied load and the minimum buckling load. For the buckling constraint not to be critical, r_B must satisfy

$$r_B < \mathrm{KDF}/\mathrm{SF} \tag{3}$$

Finally, the static and dynamic responses and the skin strains are fed into the optimizer as objective or constraint, and a gradient-based optimizer is used to update the set of lamination parameters and thickness until a converged solution is found. Feasibility constraints are used to ensure that the lamination parameters represent a feasible laminate. Constraints proposed by Hammer et al. [48] are used to ensure that in-plane and the out-of-plane lamination parameters form a feasible design space separately. Additional constraints proposed by Raju et al. [49] and Wu et al. [50] are used to relate the in-plane and the out-of-plane lamination parameters to each other.

III. Jig Shape Design and Cruise Shape Constraint

The current Paper considers only mass minimization; aerodynamic performance of the wings such as drag at cruise conditions is not explicitly considered, which can lead to overoptimistic results, because in cruise conditions aerodynamic performance, rather than structural efficiency, drives the wing design. Therefore, the cruise

shape requirement is included in the optimization as one of the constraints. In this way, the aerodynamic performance of the wing is not compromised by aeroelastic tailoring aimed at structural mass minimization or passive load alleviation.

Introduction of the cruise shape constraint has implications for the jig shape of the wing and on the optimization process. The two shapes are related through the cruise loads and the wing stiffness. Therefore, the wing stiffness is defined a priori if both the jig shape and the cruise shape are fixed. From the optimization point of view, this leaves the optimizer no freedom to exploit composite tailoring for passive load alleviation to minimize the optimization objective, namely, the structural mass of the wing. Hence, in an ideal case, the jig shape should be allowed to adjust freely during the optimization process to satisfy the cruise shape constraint, as well as to apply composite tailoring for passive load alleviation, as illustrated in Fig. 2.

A clear distinction has to be made between linear and nonlinear optimization problems. If the deformations of the wing remain small, then the optimization problem can be considered linear, and retrieval of the jig shape from the cruise shape is rather straightforward. In a simplified case, with a single cruise load case, it suffices to invert the $1g$ loads on the wing in cruise shape and perform structural analysis to obtain the corresponding jig shape. The inversion of loads works because the wing stiffness is independent of structural deformations in the linear analysis. In the nonlinear case, with larger wing deformations, the jig shape retrieval is more complex because the wing stiffness in cruise shape differs from that in the jig shape, due to geometric effects. A quasi-Newton procedure could be used in that case, as was demonstrated by Stodieck et al. [3]. When the wing structural model is geometrically nonlinear and the wing deformations are large, the previously mentioned quasi-Newton method would theoretically still work. Regardless of the nature of the optimization problem, it is important to point out that load inversion only works if the jig shape is to be retrieved from a single load case, which is usually not the case. The authors propose a more robust method in which the jig shape becomes an integral part of the optimization process. Rather than retrieving the jig shape a posteriori, the jig shape parameters become actual design variables, while the cruise shape of the wing is enforced as a design constraint. The main advantage of this approach is that the jig shape is an inherent part of the optimization process, which would allow for the optimization of an aeroelastically tailored wing, while taking into account the aerodynamic performance across a range of flight conditions and not necessarily a single cruise condition.

In the current case, the cruise shape constraint and the jig shape of the wing are defined by their respective twist distributions along the wing span. Wing out-of-plane deflection and dihedral are neglected because their influence on the wing loads and drag is relatively small in comparison to the wing twist. A cruise shape constraint is imposed on the total spanwise twist distribution of the wing at cruise conditions, which is calculated as the sum of the jig shape twist and the elastic twist deformation due to the applied external loads, such as aerodynamic forces, engine thrust, and weight due to nonstructural masses. The cruise shape constraint is satisfied if the total twist of the wing falls within the predefined bounds of the required wing twist in cruise conditions.

From the implementation standpoint, the cruise shape constraint and the jig shape are parameterized by their respective twist values at the structural nodes of the beam model representing the wing. From the algorithmic standpoint, the jig twist θ_{jig} is implemented in the optimization as follows. First, an undeflected and untwisted wing is initialized. Then, the stiffness distribution stemming from either an initial guess or previous design iteration is applied across the wing according to the specified design regions. Next, the jig twist θ_{jig} is imposed as spanwise rotation at the structural nodes, without prestressing the wing. Finally, an aeroelastic model of the wing is assembled and analyzed using the selected design load cases, including the cruise load case to evaluate the cruise shape constraint. The flow chart of the analysis process is depicted in Fig. 3, while more details regarding the implementation are available in the work by Werter [44], De Breuker et al. [51], and Werter et al. [52]. In this way, the cruise shape constraint and the jig shape become integrated into the optimization. Moreover, jig shape also becomes available as part of the optimization result; hence, no jig shape needs to be retrieved a posteriori.

Jig shape being an integral part of the optimization process has three important additional advantages. First, the sensitivities of the mass minimization objective and the sensitivities of the cruise shape constraint with respect to the jig twist design variables θ_{jig} can be calculated analytically, thereby allowing an efficient optimization process. Second, this approach can also be used when dealing with large nonlinear deformations. Third, additional constraints can be seamlessly imposed on the jig shape to satisfy possible manufacturing or other practical constraints.

A raw jig shape determined during the optimization process can exhibit peculiar behavior, such as shown at a spanwise location of around 0.5 m depicted in Fig. 4a, in which the raw jig twist suddenly undergoes a nonsmooth change in value. Such behavior is linked to the way in which the cruise shape constraint is implemented. In the current approach, the cruise shape is enforced with a margin of ± 0.05 deg around the prescribed cruise twist, which allows the cruise shape to pivot between the upper and lower limits as shown by the optimized cruise twist in Fig. 4b. The nonsmooth changes in the jig shape correspond to the transitions of the cruise twist from the lower bound to the upper bound and vice versa. Hence, two additional postprocessing steps are needed to smooth out the final jig twist:

1) The difference between the resulting cruise twist, indicated by the dashed line, and the required reference twist, indicated by the solid line in Fig. 4b, is calculated and subtracted from the optimized jig shape. The resulting corrected jig shape is indicated by the circular markers in Fig. 4a. The corrected jig twist is clearly improved in terms

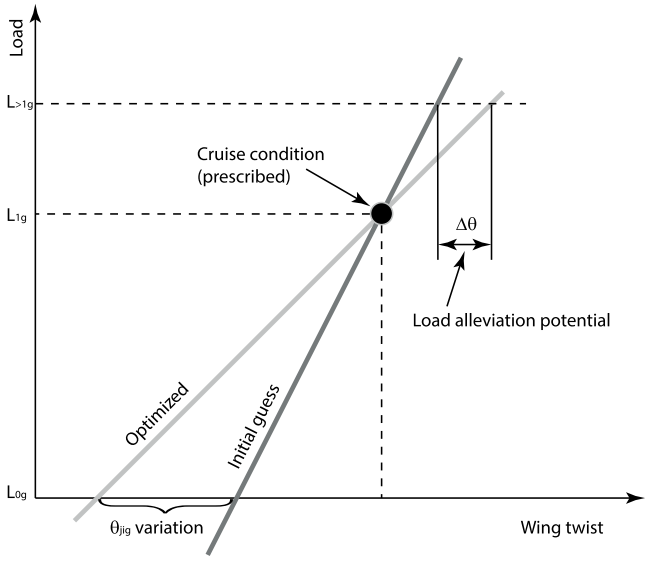

Fig. 2 Load alleviation mechanism through jig twist optimization.

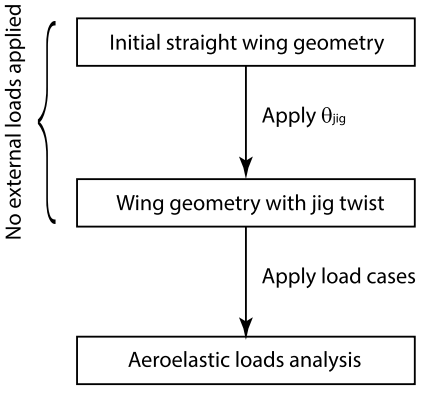

Fig. 3 Jig shape optimization process.

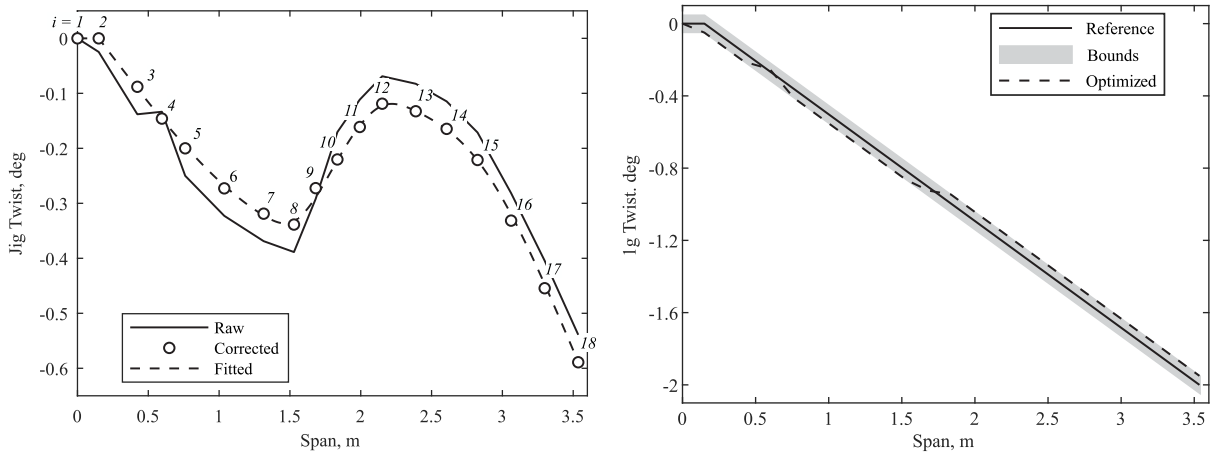

a) Jig twist **b) Cruise shape constrain implementation**

Fig. 4 Jig shape recovery.

Table 1 Smoothing spline fitting parameters

Wing	Smoothing, p	Fitting weights, w_i
Reference	0.6	10^4 $i = 14$ 10^3 $i = 2, 13, 15, 18$ 1 else
Tailored	0.75	10^4 $i = 13$ 10^3 $i = 2, 5, 6, 7, 11, 12, 15, 18$ 1 else

of smoothness. Most of the nonsmooth changes, such as the one observed at spanwise location 0.5 m, are removed. Nonetheless, small oscillations can still be observed.

2) A smoothing spline is fitted to the corrected jig twist to obtain the final jig twist shown by the dashed line in Fig. 4a. The smoothing spline is constructed using a MATLAB® fit function with the smoothingspline option enabled. The smoothing spline is obtained by minimizing

$$p\sum_i w_i(\theta_{\text{jig},i} - \theta_{\text{fit}}(y_i))^2 + (1-p)\int\left(\frac{d^2\theta_{\text{fit}}(y)}{dy^2}\right)^2 \mathrm{d}y \qquad (4)$$

where $\theta_{\text{jig},i}$ represents the jig twist at given spanwise location y_i, $\theta_{\text{fit}}(y)$ represents the cubic spline, p represents the smoothing parameter, and w_i represents the fitting weights for each data point. The parameter values used for each wing type are summarized in Table 1.

IV. Design Setup

A set of design requirements was defined by the FLEXOP project to ensure that the developed wing designs are comparable to each other and flight worthy and that the same airframe could be used for flight testing at a later stage of the project. The main design requirements defined the wing planform properties such as span, sweep angle of the leading edge, spanwise chord and airfoil distribution, control surface layout, structural layout in terms of the number of spars and ribs and their position in the wing, and the number of laminate design regions. Also defined are laminate properties such as laminate definitions, material stiffness properties, allowables and knockdown factors, trim and operating conditions in terms of aircraft total mass, flight speed, altitude and load case selection, and corresponding safety factors. The main design requirements are discussed in the following, while the complete set of design requirements and constraints is summarized in Tables A1 and A2.

Wing geometrical properties, including the cruise shape twist requirements and structural layout, are summarized in Table 2 and Fig. 5.

The structural layout is chosen in the form of a wing box. The leading edge part is excluded from the structural design as part of the load-carrying structure, because it only acts as an aerodynamic fairing. Nevertheless, the area of the leading edge should be kept as small as possible to minimize its effect on the aeroelastic response of the wing. The wing box must also house the control surface actuators and instrumentation, such as fiber Bragg and acceleration sensors to monitor the wing deformation and motion. Finally, the wing box should resemble the size of a conventional wing box used in a typical commercial aircraft. Therefore, a maximum possible size of the wing box was chosen. The front spar was located at 15% chord, and the rear spar was located at 71% chord.

The rib distribution, as shown in Fig. 5, is governed by three factors: 1) wing–fuselage interface, 2) control surface and actuator layout, and 3) the buckling behavior of the load-bearing skins. To be able to use the same airframe and flight-systems architecture, all the wing designs considered in the FLEXOP project must feature the same wing–fuselage interface and control surface layout, which determine the location of the ribs in the wing–fuselage connection area, at the root of the wing, and at the locations of the control surface actuators. Each actuator is enclosed by two ribs, which can be observed in an irregular pattern of the rib spacing, with a pair of ribs positioned close to each other, in Fig. 5. The rib pitch also affects the buckling behavior of the wing box by breaking the load-bearing skins into smaller panels. Generally, for given thickness and stiffness properties of a panel, the smaller the panel, the larger the buckling load it can support. Hence, it was decided to cluster the ribs closer together at the root of the wing, where the in-plane loads are higher, and spread them further apart toward the tip of the wing.

The laminates were designed using a standard carbon-fiber-epoxy unidirectional prepreg $C8552S/34\%/UD134/AS4$. This material was chosen for its availability and good tailoring capabilities (high ratio between longitudinal and lateral stiffness). Furthermore, the use of prepreg allows for accurate reproduction of ply angles during the laminate assembly in the forming tool. The laminate itself was constrained to a minimum thickness of 1 mm and a maximum of 12.7 mm. The minimum thickness constraint was chosen to ensure minimum robustness in terms of handling qualities during the manu-

Table 2 Wing geometry

Parameter	Value
Semispan, m	3.536
Chord, root/tip, m	0.471/0.236
Airfoil thickness, root/tip,[a] % chord	10/8
Sweep, leading edge, deg	20
Cruise shape twist, root/tip,[a] deg	0/−2

[a]Linearly decreasing from root to tip.

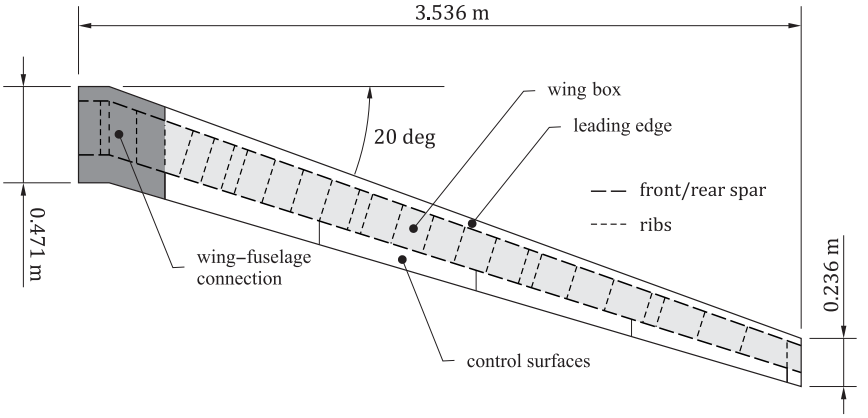

Fig. 5 Wing structural layout.

facturing process. The maximum thickness was chosen to be large enough for this constraint not to become active during the optimization process, in order to allow the optimization process to always find a feasible solution.

The reference wing is confined to symmetric-balanced laminates, while the tailored wing is composed of symmetric-unbalanced laminates. The difference in laminate definition is the only difference in the definition of the optimization problem for the two wing designs.

Because of the manufacturing requirements, the material reference axis, namely, the orientation of the 0 deg plies, has to be aligned with either the front or the rear spar. However, it is well known that the aeroelastic tailoring capabilities of symmetric-balanced laminates depend on the selection of the material reference axis [19]. The influence of the selection of the material reference axis is illustrated in Fig. 6. In the case of the reference wing, a slightly larger mass reduction was obtained with the material reference axis aligned with the rear spar in comparison to aligning it along the front spar. Hence, the direction along the rear spar was chosen as the material reference axis. Nevertheless, it is important to keep in mind that potentially better results could be achieved if the material reference axis were allowed to assume an arbitrary direction.

In terms of operating and trim conditions, all the load cases are evaluated at a cruise speed of 45 m/s at an altitude of 800 m above sea level. The trim condition for all load cases was defined as

$$L = ngm \tag{5}$$

where L, m, n, and g represent lift, aircraft mass, load factor, and the gravitational acceleration.

In addition to the $1g$ cruise load, positive and negative limit loads are defined in the design process at $5g$ and $-2g$, respectively. Positive and negative limit loads are set to different load factors according to how the airplane will be operated during testing. To demonstrate load alleviation, only maneuvers with positive load factor are envisaged, whereas maneuvers with negative load factors are to be avoided. Besides, because of the asymmetric shape of the selected airfoil, it is expected that the aircraft cannot achieve negative loads as great in magnitude as the positive loads.

Safety requirements are imposed in terms of a prescribed safety factor and knockdown factors applied to the material allowables. The safety factor is set at 1.5. This way, a sufficient margin between the limit and the ultimate load is guaranteed.

Both strength and stiffness properties of composites are well known to be susceptible to manufacturing inaccuracies, environmental changes, and damage during part manufacturing and service life [53]. Hence, the actual individual property values can depart significantly from the nominal values provided by the material manufacturer. It was decided to use the B-basis knockdown for material scatter, the 90 deg/wet knockdown for environmental effects, and the knockdown for the barely visible damage that might occur during service to ensure structural strength of the designed wings.

Stiffness properties used in the calculation of the aeroelastic response were not subject to any knockdown factors, and the mean stiffness values were used directly. However, a B-basis knockdown was applied to the stiffness properties in the evaluation of the critical buckling load, to provide a sufficient margin of safety.

The control surface layout is shown in Fig. 5. To ensure sufficient controlability of the aircraft, the minimum acceptable control effectiveness, as defined by Eq. (1), was set to 0.15, which corresponds to a roll rate of 19.2 deg/s in cruise and 8.2 deg/s in landing conditions at a 10 deg aileron deflection, respectively. Aileron deflection assumes that all three ailerons are deflected by the same amount in an antisymmetric fashion on the starboard and port sides of the wing.

Finally, the laminate comprising the wing is optimized in spanwise uniform patches called design regions. Within each design region, a set of lamination parameters and laminate thickness are optimized with the objective of reducing the overall structural mass of the wing. The wing is split into 12 spanwise design regions along the span, as shown in Fig. 7. The number of chordwise design regions is restricted to 1 due to manufacturing limitations.

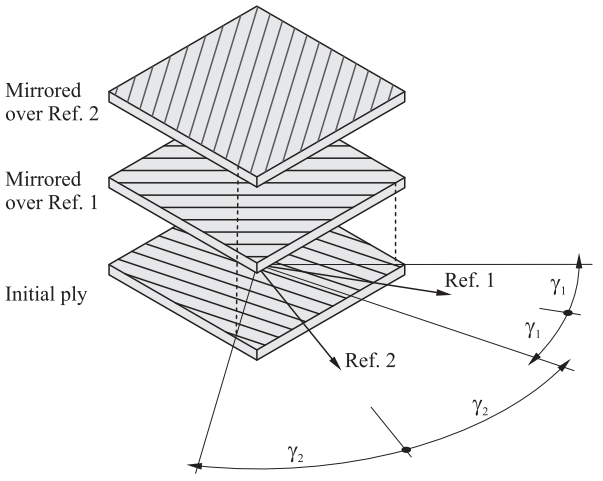

Fig. 6 The effect of reference material axis on a balanced laminate.

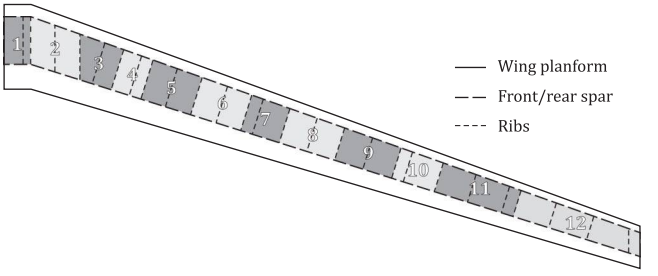

Fig. 7 Design region distribution.

V. Results

The comparison between the reference and the tailored wing is presented in this section. First, design parameters such as jig twist, stiffness distribution, thickness, and structural weight are compared, followed by a comparison of the aeroelastic response under the selected design load cases. The aeroelastic response is analyzed in terms of aerodynamic properties, root loads, and wing deformations. In addition, important design constraints are also discussed within the scope of the aeroelastic response.

A. Design Parameters

The design of the reference and tailored wings resulting from the optimization process are compared in this section. The compared design parameters are jig twist, membrane and bending stiffness distributions, and thickness distribution in the wing skins and spars along the wing span. The observed differences and trends are explained using the aeroelastic response of the designed wings to a set of selected load cases.

1. *Jig Twist*

The optimized raw and the final smoothened jig twists of the reference and the tailored wing are compared in Fig. 8. Two main differences can be observed between the reference and the tailored wing. First, the jig twist of the reference wing is, in general, much larger than that of the tailored wing. In the case of the reference wing, the wing tip has a jig twist of −1.38 deg, whereas the tip of the tailored wing has a jig twist of only −0.59 deg. Second, the jig twist of the reference wing decreases monotonically along the span from root to tip. On the other hand, the jig twist of the tailored wing exhibits nonmonotonic behavior; initially, the jig twist is decreasing up to a spanwise location of 1.5 m, and then it starts to increase up to the spanwise location of 2.3 m, when it starts to decrease again to the tip of the wing. The observed differences are explained by the difference in the imposed laminate constraints. Unlike the symmetric-unbalanced laminates used in the tailored wing, the symmetric-balanced laminates comprising the reference wing cannot exhibit any extension–shear or bend–twist coupling. Consequently, in the case of the reference wing, the bending moments resulting from the aerodynamic loads cannot induce any torsional deformation due to the lack of aforementioned material coupling. As a result, more twist has to be built into the jig shape of the reference wing to meet the 1g shape requirement. It is interesting to note that Brooks et al. [5] obtained a jig shape similar to the jig shape of the tailored wing during their aeroelastic optimization of a tow-steered composite wing using a high-fidelity integrated design approach.

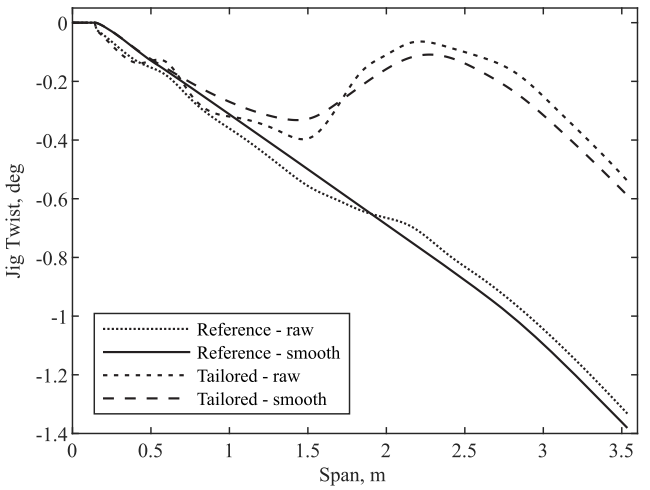

Fig. 8 Comparison between raw and smooth jig twist.

The effect of the smoothing process is clearly observable in Fig. 8. The amount of required smoothing is shown in Sec. III to correspond to the cruise shape constraint margins, which are set at ±0.05 deg. To investigate the effect of the smoothing process, and thereby the cruise shape constraint margins, on the aerodynamic performance of the two wings, the lift distribution in 1g cruise load is compared in Fig. 9a for both the raw and the smooth jig shapes for both wing types. One can hardly discern between the different lift distributions. The maximum relative difference in lift distribution between the raw and smooth jig twist for both wings is less than 2.5%, as shown in Fig. 9b. The observed differences are small enough to consider the smoothing process to have a negligible effect on the aerodynamic performance of the two wings in cruise conditions, which also indicates that the cruise shape constraint margin of ±0.05 deg is sufficiently tight.

2. *Stiffness Distribution*

Stiffness properties of the optimized reference and tailored wing can be compared in two ways. One can compare membrane and bending stiffness of the laminates per design region in each individual structural member of the wing such as wing skins and spars, or one can compare the stiffness properties of the corresponding Timoshenko beam models.

In the first case, stiffness properties of each design region are visualized as a polar representation of the membrane and bending thickness-normalized engineering moduli of elasticity, $E_{11}^{A}(\theta)$ and $E_{11}^{D}(\theta)$, respectively. The visualization technique was introduced by Werter [44] and Dillinger [54] as

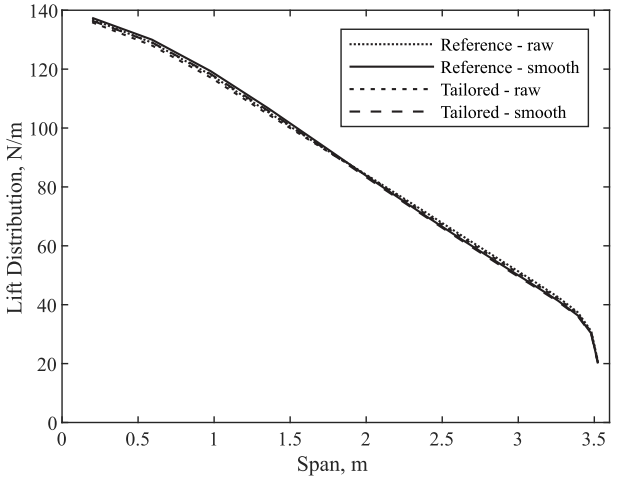

a) Lift distribution in 1 g load case

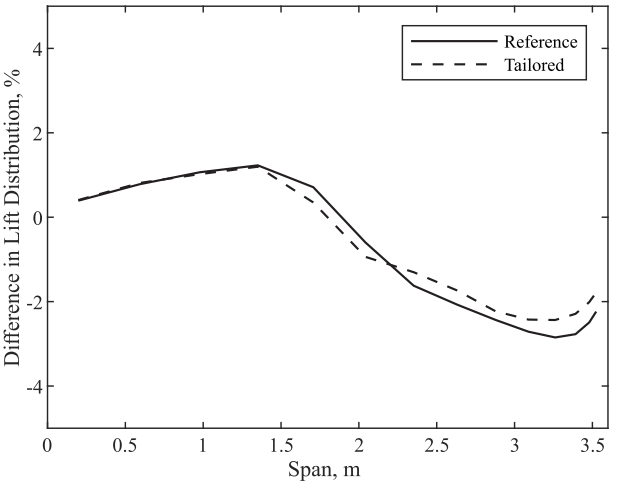

b) Difference in the lift distribution between raw and smooth jig shape

Fig. 9 The effect of jig twist smoothing on the lift distribution in 1g load case.

$$E_{11}^{A}(\theta) = 1/\left(\hat{\boldsymbol{A}}_{11}^{-1}(\theta)\right)$$
$$E_{11}^{D}(\theta) = 1/\left(\hat{\boldsymbol{D}}_{11}^{-1}(\theta)\right) \tag{6}$$

where

$$\hat{\boldsymbol{A}}^{-1}(\theta) = \boldsymbol{T}^{T}\hat{\boldsymbol{A}}^{-1}\boldsymbol{T}$$
$$\hat{\boldsymbol{D}}^{-1}(\theta) = \boldsymbol{T}^{T}\hat{\boldsymbol{D}}^{-1}\boldsymbol{T} \tag{7}$$

and

$$\boldsymbol{T} = \begin{bmatrix} \cos^2\theta & \sin^2\theta & 2\cos\theta\sin\theta \\ \sin^2\theta & \cos^2\theta & -2\cos\theta\sin\theta \\ -\cos\theta\sin\theta & \cos\theta\sin\theta & \cos^2\theta - \sin^2\theta \end{bmatrix} \tag{8}$$

where $\hat{\boldsymbol{A}}$ and $\hat{\boldsymbol{D}}$ are the membrane and bending thickness-normalized laminate stiffness matrices. Matrix $\boldsymbol{T}$ is the axes transformation matrix.

In the second case, the Timoshenko cross-sectional stiffness matrix $\boldsymbol{C}$ obtained using the cross-sectional modeler [45] relates the cross-sectional strains and curvatures to forces and moment:

$$(F_1, F_2, F_3, M_1, M_2, M_3)^T = \boldsymbol{C} \cdot (\varepsilon_{11}, \varepsilon_{12}, \varepsilon_{13}, \kappa_1, \kappa_2, \kappa_3)^T \tag{9}$$

In the current case, one is mainly interested in bending stiffness EI, torsional stiffness GJ, bend–twist coupling K, and shear center location e, which are related to the Timoshenko stiffness and compliance matrices $\boldsymbol{C}$ and $\boldsymbol{C^{-1}}$ as

$$EI = C_{55}$$
$$GJ = C_{44}$$
$$K = -C_{45}$$
$$e = -C_{34}^{-1}/C_{44}^{-1} \tag{10}$$

Membrane and bending stiffness distributions along the span of the reference and tailored wings are compared for each structural member in Fig. 10, with the corresponding lamination parameters and laminate thicknesses summarized in Tables B1 and B2. The resulting beam stiffness properties are shown in Fig. 11.

Membrane stiffness distributions for the top and bottom skin and the spars are shown in Figs. 10a, 10c, and 10e. In the wing skins, one can identify three distinct tailoring regions: the root, the central, and the wing-tip region. For both the reference and the tailored wings, prominent membrane stiffness tailoring is only present in the central region, while tailoring is less evident in the root and tip regions. The membrane stiffness in the central part is highly anisotropic with the dominant stiffness directions oriented diagonally forward with respect to the wing reference axis, to promote washout deformation of the wing when bending. As expected, the stiffness anisotropy is much more pronounced in the tailored wing due to the difference in the laminate constraint between the two wings. Finally, as shown in Fig. 10e, the membrane stiffness is only weakly tailored in the spar members of both wings, which is indicated by a nearly circular polar representation of $E_{11}^{A}(\theta)$.

Bending stiffness distributions for the top and bottom skin and the spars are shown in Figs. 10b, 10d, and 10f, respectively. Tailoring of the laminate bending stiffness is considerably more pronounced for all wing box members of both wings. Again, the laminate tailoring is more prominent in the tailored wing, which results in the polar representation of $E_{11}^{D}(\theta)$ dominated by a specific stiffness direction. On the other hand, in the reference wing, there always exists an equally prominent conjugate stiffness direction with respect to the defined material axis, due to the balanced laminate constraint. The material axis is aligned with the beam reference axis along the rear spar of the wing. As for the membrane stiffness, one can identify three distinct tailoring regions in the top and bottom skins for both wing types. At the root of the wing, the tailoring process yields laminates having the primary stiffness orientation along or slightly aft of the material axis. In the central region, the laminate stiffness is oriented diagonally forward. In the tip region, the laminate stiffness is symmetric around the material axis which coincides with the wing reference axis.

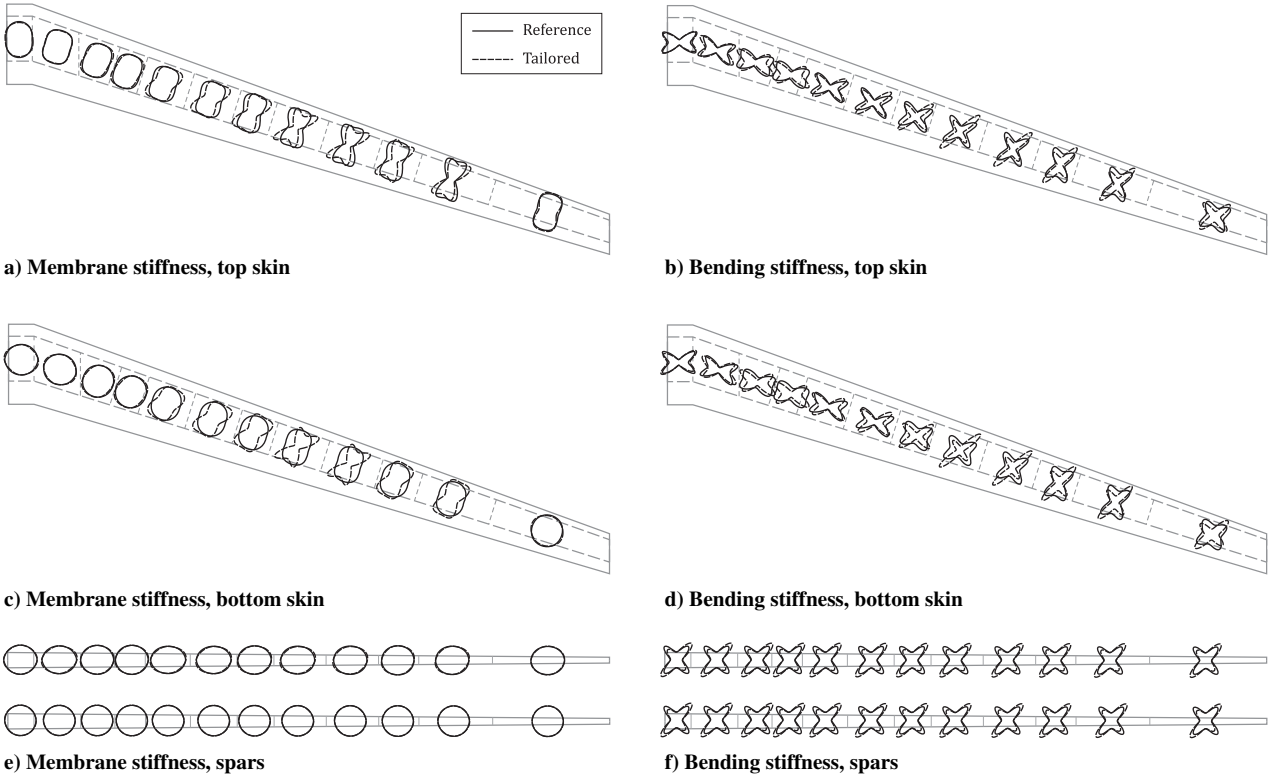

a) Membrane stiffness, top skin

b) Bending stiffness, top skin

c) Membrane stiffness, bottom skin

d) Bending stiffness, bottom skin

e) Membrane stiffness, spars

f) Bending stiffness, spars

Fig. 10 Comparison of composite tailoring between the reference and the tailored wing.

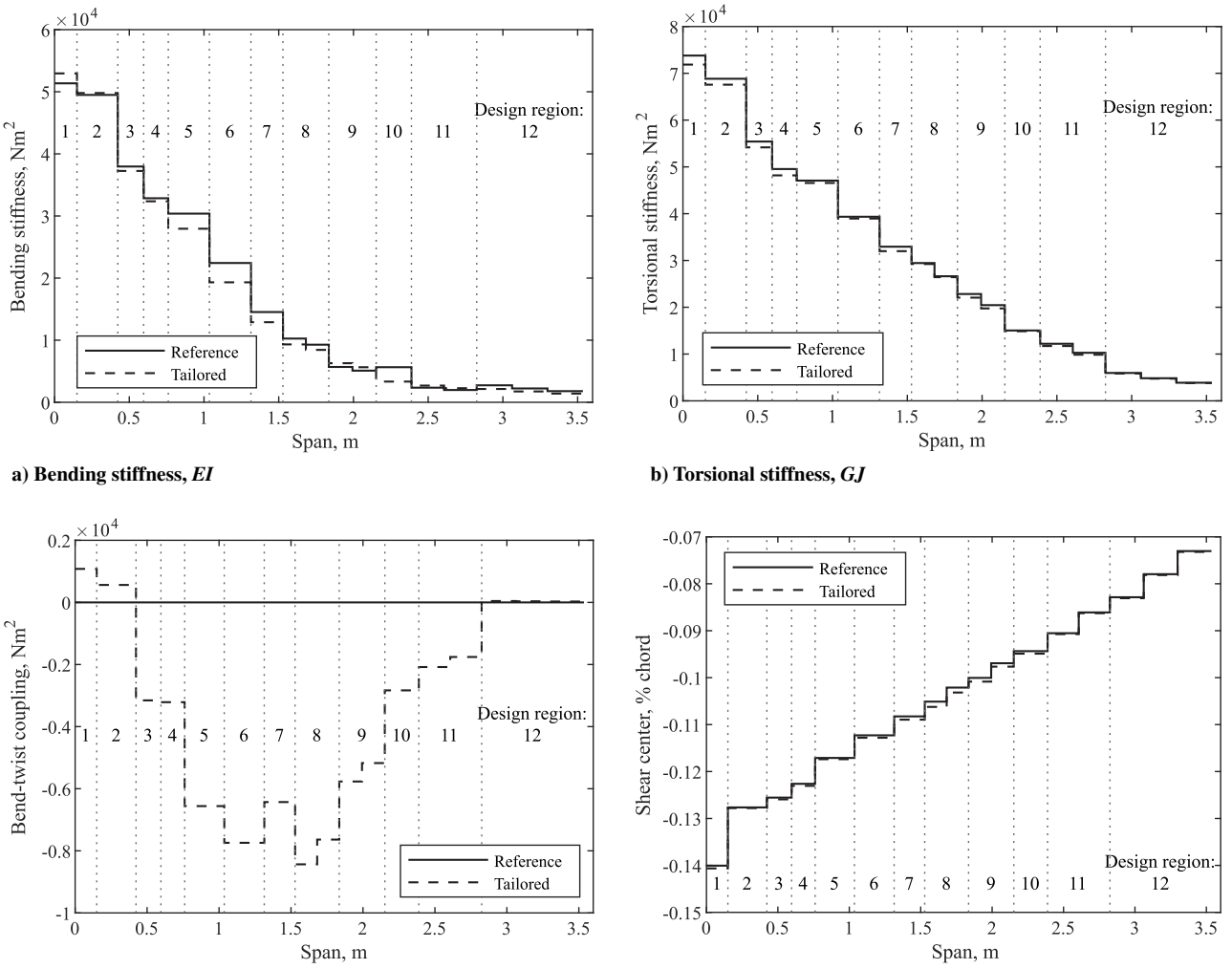

a) Bending stiffness, *EI*

b) Torsional stiffness, *GJ*

c) Bend-twist coupling, *K*

d) Shear center, 4 *e*

Fig. 11 Comparison of equivalent Timoshenko beam properties between the reference and the tailored wing.

The observed differences in the membrane and bending stiffness distributions reflect also in the beam stiffness properties. According to Fig. 11, the largest differences between the reference and the tailored wing are found in *EI* and *K*. The tailored wing is more flexible in bending in the central part of the wing, in the design regions 5 to 8. In terms of *K*, the reference wing exhibits no bend–twist coupling, as expected due to the use of symmetric-balanced laminates. On the other hand, the tailored wing exhibits strong bend–twist coupling. The bend–twist coupling in design regions 1 and 2 is positive, which promotes wash-in deformations. The bend–twist coupling in design regions 3 to 11 is negative, which leads to a washout deformation. Finally, the bend–twist coupling in design region 12 is almost zero. In this sense, the spanwise distribution of the bend–twist coupling also reflects the three tailoring regions observed in the membrane stiffness distributions presented in Fig. 10. The observed behavior of the bend–twist coupling is also as to be expected of the outcome of an optimization with passive MLA as an objective, where loads are reduced on the outboard section of the wing by the washout deformation and attracted to the in-board section of the wing by the wash-in deformation. Finally, the differences in *GJ* and *e* of the two wings are very small. In this regard, the two wings appear to have almost identical properties.

3. *Thickness Distribution*

The thickness distributions of the laminates comprising the top skin, bottom skin, and the spars are compared in Fig. 12. Similar thickness distribution in the top and bottom skin is observed for both wings. The optimized bottom skin is thinner than the top skin due to the less severe maximum negative load case in comparison to the maximum positive load case. It is also observed that for both wings both the front and the rear spar are of a constant thickness of 1 mm, which equals to the minimum laminate thickness constraint.

There is a noticeable difference in the thickness of the wing skins between the reference and the tailored wing, which is attributed to the greater tailoring freedom of the symmetric-unbalanced laminates used in the tailored wing in comparison to the symmetric-balanced laminates used in the reference wing.

Furthermore, the difference in skin thickness between the two wing types differs significantly for the top and the bottom skins. The difference in the top skin thickness is on average 0.08 mm, while there is on average a difference of 0.14 mm in the bottom skin thickness. The relative difference between individual skins is shown in Fig. 12b.

The resulting mass comparison is summarized in Table 3. Structural mass accounts only for the material mass of the wing box. The total mass accounts for all other masses installed in the wing, such as ribs, control surfaces, actuators, paint, and sensors in addition to the structural mass of the wing box. It is important to point out that both structural and total mass are expressed for the entire wing span. Finally, the aircraft mass accounts for the total mass of the aircraft, including the mass of the fuselage and the empennage.

The difference in skin thickness between the reference and the tailored wing results in a 4% structural mass reduction in favor of the tailored wing. Because the structural mass of the wing represents only a fraction of the total aircraft mass, the overall mass reduction on the aircraft level diminishes to about 1%. The structural mass reduction of 4% agrees well with the trends observed by Stanford et al. [8], who

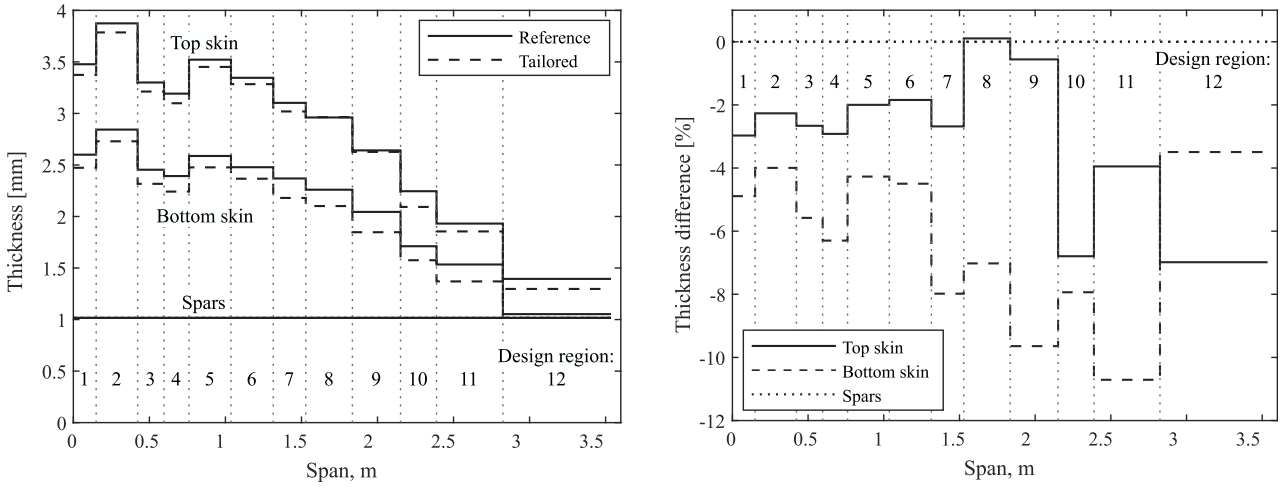

a) Laminate thickness **b) Laminate thickness comparison**

Fig. 12 Laminate thickness distribution along the wing span.

Table 3 Mass comparison

Wing	Structural mass,[a] kg	Total mass,[b] kg	Aircraft mass,[c] kg
Reference	11.8	24.1	65.4
Tailored	11.3 (−4%)[d]	23.7 (−2%)[d]	64.9 (−1%)[d]

[a]Structural mass of the wing skins and spars.
[b]Wing structural and nonstructural mass such as mass of the cabling, actuators, and sensors.
[c]Aircraft structural and nonstructural mass.
[d]Relative difference with respect to the reference wing.

observed a 4.56% mass reduction of symmetric-unbalanced design relative to the symmetric-balanced design.

B. Aeroelastic Response

This section presents the aeroelastic response of the reference and the tailored wing for the $1g$, $5g$, and $-2g$ load case. First, aerodynamic characteristics such as lift and local angle of attack distribution are presented and summarized in terms of cumulative root loads. Then, the structural response is reviewed in terms of out-of-plane and torsional deformation of the wings, followed by a discussion of the structural constraints.

1. Aerodynamic Response

The lift distribution for the reference and the tailored wing is shown in Fig. 13. First, both wings exhibit almost identical lift distribution in the $1g$ load case, which results from enforcing the cruise shape constraint in terms of wing twist. Second, there is a significant difference in the lift distribution between the two wings in the 5 and $-2g$ load cases due to the presence of the extension–shear and bend–twist coupling in the laminates comprising the tailored wing. This coupling enables the tailored wing to redistribute the aerodynamic loads toward the root of the wing by affecting the wing twist. The spanwise location of the center of pressure for both wings is at 42.8% of the span in the $1g$ load case. In the $5g$ load case, the spanwise location of the center of pressure moves to 47.4 and 44.5% of the span for the reference and the tailored wing, respectively. Similarly, in the $-2g$ load case, the spanwise location of the center of pressure for the reference wing moves to 51.2% of the span and 45.6% of the span for the tailored wing. There is a larger difference between the two wings in the $-2g$ load case, which is explained by the difference in the jig shape of the two wings. The reference wing requires considerably more washout built into the jig shape to satisfy the cruise shape constraint, which leads to increased outboard loading of the wing in the negative load cases. This is also confirmed by the comparison shown in Fig. 13b.

A comparison of the local angle of attack is shown in Fig. 14. As expected, the two wings exhibit an almost identical angle of attack distribution along the span in the $1g$ load case, which indicates that the 4% difference in structural mass between the two wings has a negligible effect on the angle of attack. Moreover, the local angle of attack indicates that both wings closely follow the required $1g$ twist distribution, namely, that the local angle of attack should decrease linearly by 2 deg from root to tip.

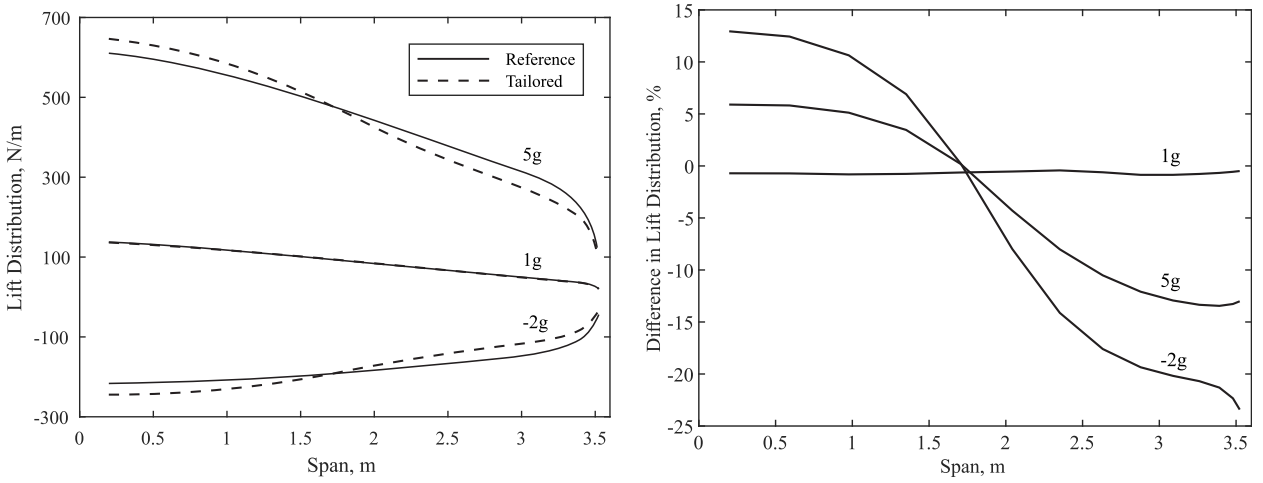

a) Lift distribution **b) Comparison of the lift distribution**

Fig. 13 Lift distribution in design load cases.

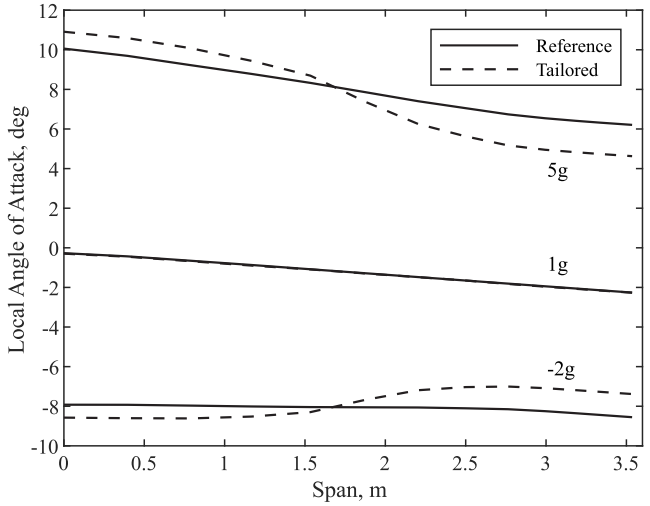

Fig. 14 Local angle of attack along the span in trimmed flight in the design load cases.

The local angle of attack in the $5g$ and $-2g$ load cases reflects the expected behavior the wings tailored for MLA. The local angle of attack of the tailored wing is larger in the inboard section and smaller in the outboard section of the wing in comparison to the reference wing, which corresponds to the differences observed in the lift distributions presented in Fig. 13.

It is noteworthy that the angle of attack at the root corresponds to the trim angle of attack for the whole aircraft. A trimmed flight condition (weight equals lift) is obtained at -0.30 deg angle of attack for both wings in the $1g$ load case, whereas in the $5g$ and $-2g$ load cases, the reference wing is trimmed at 10.1 and -7.9 deg, and the tailored wing is trimmed at 10.9 and -8.6 deg, respectively.

Finally, the root forces and moments for the two wing types are presented in Table 4. As expected, both wings exhibit almost identical shear force in the lift direction V_z and corresponding root bending moment M_x in the $1g$ load case, which indicates that the cruise shape constraint was successfully imposed on both wings. There is a noticeable difference in shear force in the spanwise direction V_y and the corresponding root bending moment M_z which is attributed to the difference in the out-of-plane deflection.

Inspecting the loads obtained in the $5g$ load case, one can observe a 6 and an 11% reduction in root bending moment M_x and torsional moment M_y, respectively, of the tailored wing relative to the reference wing, with the shear forces maintained at similar magnitudes. The reduction in both M_x and M_y is explained by the lift redistribution toward the inboard section of the wing, as observed in the case of the tailored wing in Fig. 13. Similar conclusions can be drawn for the $-2g$ load case with a reduction in M_x of 11% and a reduction in M_y of 35%.

2. Structural Response

Comparison of the aeroelastic out-of-plane and torsional deformation between the two wing types for the selected load cases is shown in Fig. 15. One can observe that the tailored wing is considerably more flexible in comparison to the reference wing. The difference in the observed tip deflection is 46% for the $1g$, 23% for the $5g$, and 8% for the $-2g$ load cases. It is interesting to note that the greatest difference in observed deflections occurs for the $1g$ load case, while the smallest difference is observed for the $-2g$ load case. In the $1g$ case, both wings experience the same aerodynamic loads, due to the cruise shape constraint. Hence, the difference in deflections reflects the real difference in the bending stiffness between the two wings. In the $5g$ and $-2g$ load cases, the exerted aerodynamic loads differ between the two wings due to the effects of composite tailoring. As the aerodynamic load distribution of the reference wing becomes more severe in comparison to the tailored wing, the difference in the tip deflection is reduced. However, for the negative load case, the difference in lift distributions is larger than for positive load cases as shown in Fig. 13; hence, the difference in the wing-tip out-of-plane deflection between the two wings is further reduced.

The difference in torsional deformation between the two wings is even larger. At the wing tip, the difference amounts to 121, 133, and 140% for the $1g$, $5g$, and $-2g$ load cases, respectively. The difference is attributed to the overall thinner skins and the bend–twist coupling present in the tailored wing.

In this context, it is interesting to break down the total twist of the investigated wings for the $1g$ load case in more detail to assess how well the wing design complies with the imposed cruise shape constraint after processing the jig shape as described in Sec. III. Figure 16 shows such a breakdown for both the reference and the tailored wing. Both wings exhibit the same total twist. According to the cruise shape constraint, the wing twist must linearly decrease from 0 deg at the root to -2 deg at the tip of the wing. The total wing twist, on the other hand, equals to the sum of jig twist, presented in Fig. 8, and the torsional deformation presented in Fig. 15b. One can observe that for both the reference as well as the tailored wing the total wing twist complies very well with the imposed cruise shape constraint. Deviations from the cruise shape constraint are slightly larger in the case of the tailored wing due to the fact that the jig shape was affected more by the postprocessing procedure detailed in Sec. III.

The second important aspect of the structural part of the aeroelastic response is the buckling and strain constraints that were imposed on the wing design during the optimization process. Figures 17 and 18 show to what extent these two constraints become critical for the selected load cases for the reference wing and the tailored wing, respectively. The buckling constraint is the more critical constraint of the two for both wing types. Most of the top and bottom skin is critical in buckling due to the high compressive loads present in the skins in the $5g$ and $-2g$ load cases. It is noteworthy that the critical value for buckling is less than 1 due to the application of the safety factor and the B-basis knockdown for material scatter, as discussed in Sec. IV.

Table 4 Comparison of the root forces and moments

Wing	V_x, N	V_y, N	V_z, N	M_x, Nm	M_y, Nm	M_z, Nm
			Load case: 1g			
Reference	0.96	−3.9	202.4	304	−93.2	−3.8
Tailored	1.04 (1.09)[a]	−5.6 (1.43)	202.4 (1.00)	305 (1.00)	−93.5 (1.00)	−5.1 (1.35)
			Load case: 5g			
Reference	−176.8	−25.5	996.4	1662	−326.5	262.8
Tailored	−191.5 (1.08)	−34.2 (1.34)	993.7 (1.00)	1555 (0.94)	−291.4 (0.89)	257.5 (0.98)
			Load case: −2g			
Reference	−55.8	6.7	−400.9	−726	76.9	98.4
Tailored	−60.4 (1.08)	10.5 (1.56)	−400.3 (1.00)	−647 (0.89)	49.9 (0.65)	95.1 (0.97)

[a]Relative to the reference wing (tailored/reference).

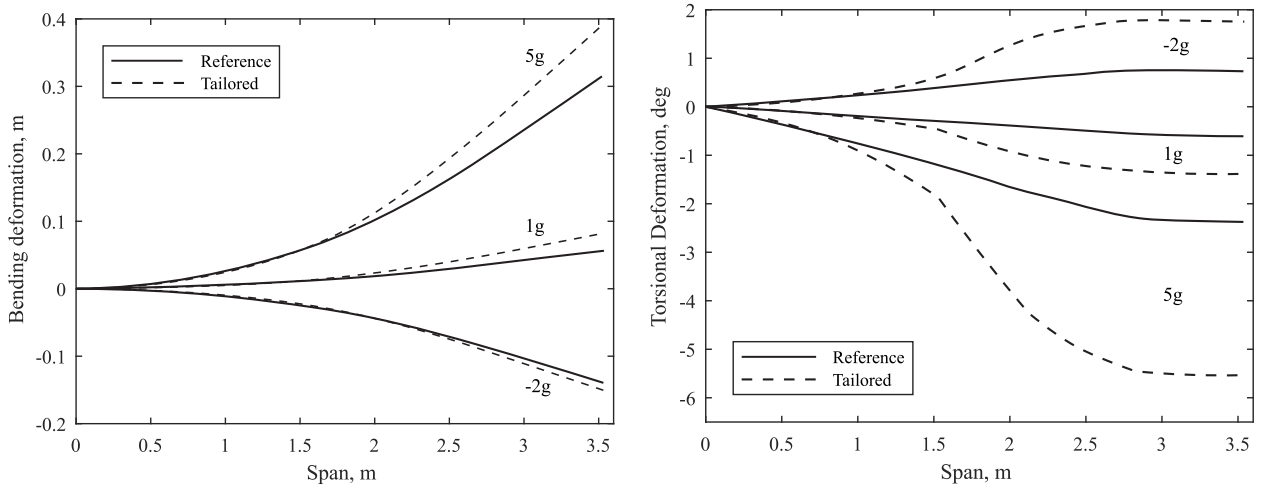

a) Out-of-plane deformation **b) Torsional deformation**

Fig. 15 Aeroelastic deformation under the design load cases.

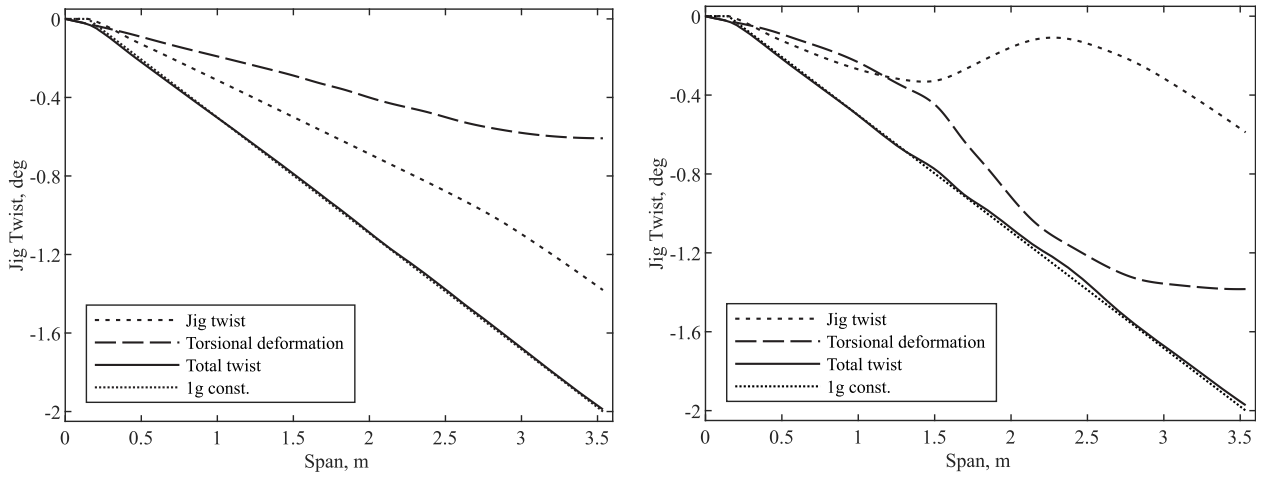

a) Reference wing **b) Tailored wing**

Fig. 16 Breakdown of total wing twist for the 1*g* load case.

Despite the relatively high wing-tip out-of-plane deflection of about 10% semispan at 5*g* and the application of the safety factor and material knockdowns, the strain constraint is not critical for either of the two wings. In the case of the reference wing, the strain coefficient does not exceed 0.25 anywhere on the wing, whereas in the case of the tailored wing the maximum strain coefficient does not exceed the value of 0.4. It is noteworthy that the relatively high strain values in the tailored wing are confined to a narrow region in the midsection of the wing in the 5*g* load case.

Finally, the spars are not critical either in buckling or strain for either of the two wings. It was shown in the preceding section that the thickness of the spars is governed by the minimum thickness constraint, which was selected for manufacturing reasons. Consequently, the spars are sufficiently stiff to easily resist buckling loads and strains.

C. Effect of Aeroelastic Response on Optimized Design

The design and the aeroelastic response of flexible aircraft wings are highly interdependent. The wing design drives the aeroelastic response and vice versa in the optimization process. Hence, the outcome of the design optimization can only be understood in conjunction with the optimized aeroelastic response. In the current Paper, the differences in the laminate tailoring patterns and the thickness distribution are interesting to consider in more detail.

The tailoring patterns observed in both membrane and bending stiffness can be explained by considering the incentives originating from the definition of the optimization problem. As shown in Figs. 17 and 18, the buckling constraint is critical over most of the two wings. The optimization process has three tailoring mechanisms to mitigate the buckling constraint: 1) increase of the buckling load of the panels by tailoring their laminate bending stiffness, 2) redistribution of structural loads within the structure by adjusting local stiffness across the structure, and 3) alleviation of the aerodynamic loads by promoting favorable extension–shear and bend–twist couplings in the laminates.

In the case of the reference wing, buckling is primarily mitigated by the first mechanism, which optimizes the bending stiffness of the laminates to increase the buckling load of the panels comprising the wing structural members. The optimal bending stiffness matrix and the ratio of its elements depend on the aspect ratio of the particular panel, the combination of applied loads, and the boundary conditions. Nevertheless, following the general design rules given by Kassapoglou [53], the buckling performance of a panel can be improved by maximizing the D_{66} term of the bending stiffness matrix, which, in terms of the ply orientations, is achieved by orienting the plies in ± 45 deg direction and placing them as far as possible from the neutral axis of the panel. Such a laminate would show a starlike stiffness pattern similar to those shown in Figs. 10b, 10d, and 10f. The second mechanism, which is mainly achieved by adjusting the membrane stiffness of the laminates, is considered of secondary importance because the laminate cannot change in the chordwise direction in the wing skins. Therefore, it is not possible to

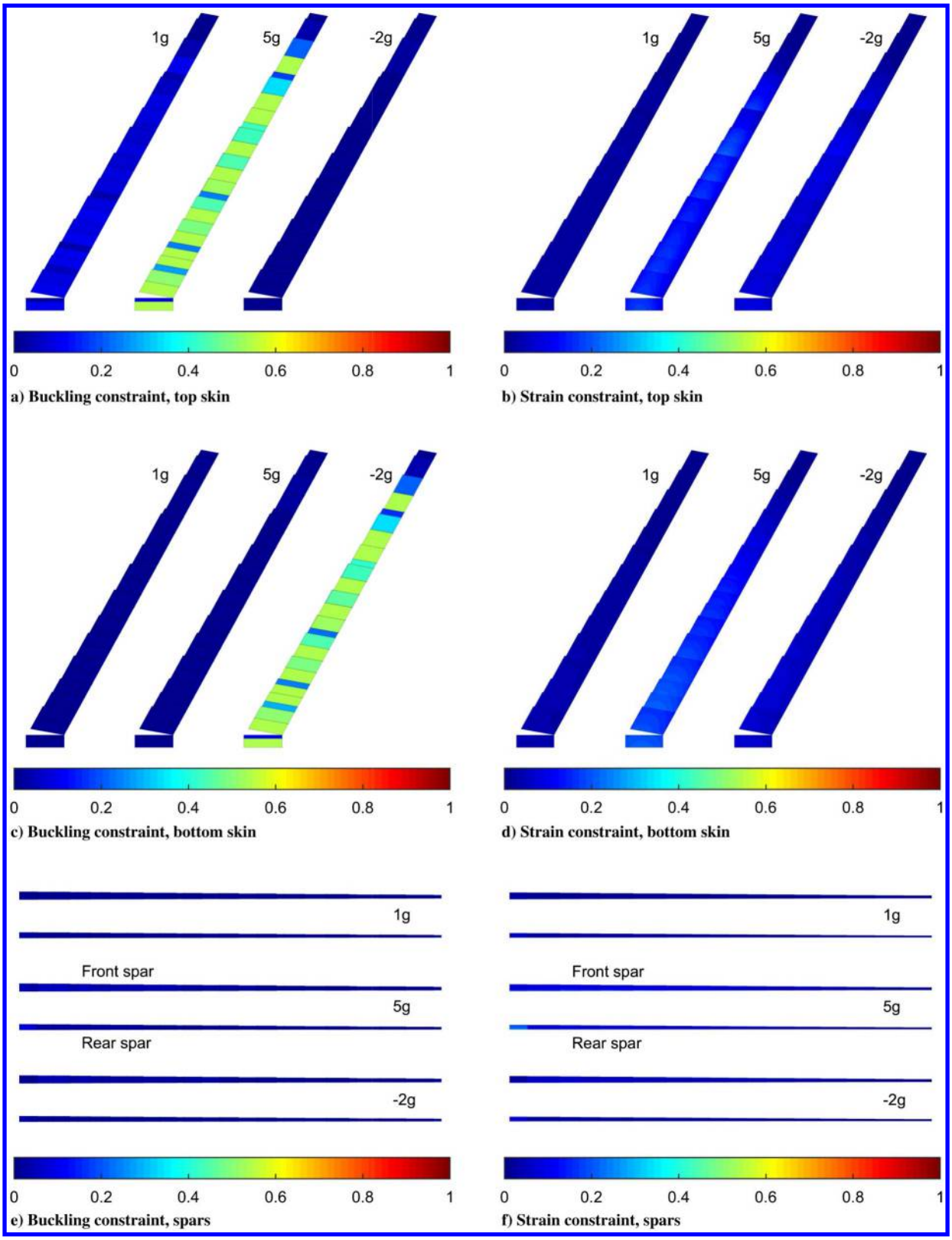

Fig. 17 Comparison of buckling and strain design constraint for the reference wing.

deflect loads away from the critical regions in the skins. The third mechanism is not possible in the reference wing due to the use of symmetric-balanced laminates. Therefore, to reduce the laminate thickness as much as possible and to save structural weight, the bending stiffness is strongly tailored across the entire wing span. On the other hand, the strain constraint, which would promote tailoring of the membrane stiffness, is not critical, as shown in Sec. V.B. Hence, for the reference wing, the degree of tailoring of the membrane stiffness is rather small across the entire wing span.

The tailored wing exhibits similar tailoring properties except in the central region between 1.5 and 2.5 m span. In the case of symmetric-unbalanced laminates, extension–shear couplings in the membrane stiffness can be used to alleviate aerodynamic loads by redistributing them closer to the wing root as shown in Fig. 13. The

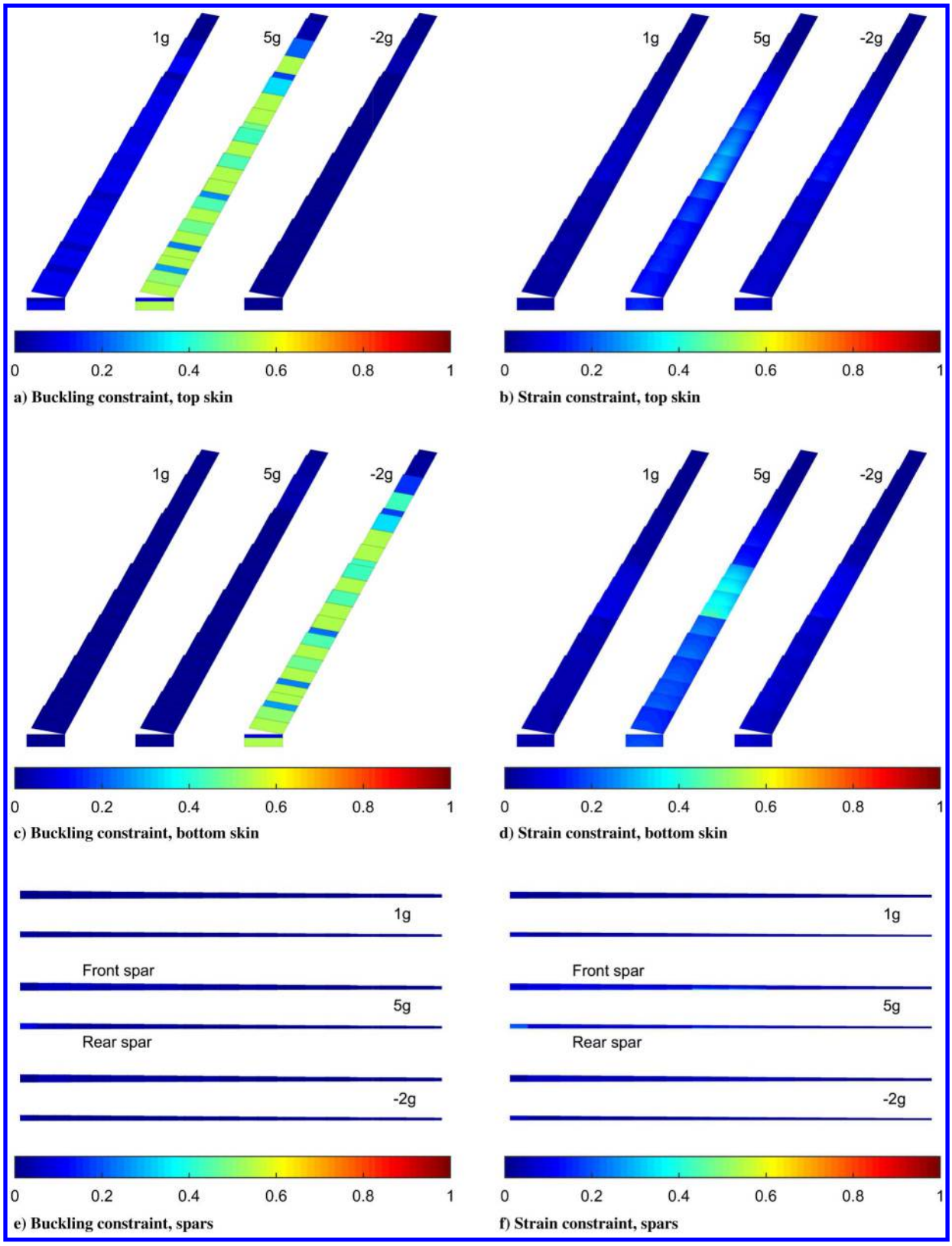

Fig. 18 Comparison of buckling and strain design constraint for the tailored wing.

result of the tailoring in the central region is thus a tradeoff between the first and the third buckling alleviation mechanisms. Hence, more prominent tailoring in membrane stiffness can be observed. Similar tailoring behavior would also be expected in the tip region of the tailored wing. However, this region undergoes little deformation in terms of strains, which results in low sensitivity of load alleviation to tailoring. Nevertheless, part of the tip section is still critical in buckling, which explains the tailoring patterns observed in the bending stiffness.

In terms of skin thickness, similar thickness distributions are observed for both the reference wing and the tailored wing in general, which is explained by identical structural layout of the spars and ribs in combination with the fact that the same constraint type, namely, buckling, drives both designs. On the other hand, the larger

differences in the thickness of the bottom skin relative to the top skin between the two wings are explained by inspecting the aeroelastic response under the $-2g$ load case in conjunction with the optimized jig twist. As shown in Fig. 8, the jig twist of the reference wing, relative to the tailored wing, exhibits considerably more washout toward the wing tip. As a result, the outboard part of the reference wing is subject to considerably higher aerodynamic loads in the $-2g$ load case, as shown in Fig. 13. Hence, the thickness of the bottom skin of the reference wing has to be considerably increased to resist the higher buckling loads. In the $5g$ load case, the jig twist of the reference wing is more favorable in terms of aerodynamic load distribution, because the wing has a considerable amount of washout already built in to its jig shape. Hence, the difference in the buckling loads resulting from the $5g$ aerodynamic loads between the two wings is smaller, which leads to smaller thickness differences in the top skin of the two wings. Nevertheless, the top skin of the tailored wing is still thinner due to the better load alleviation capabilities of the symmetric-unbalanced laminates used in the tailored wing.

VI. Conclusions

The aeroelastic analysis and design framework developed at Delft University of Technology was successfully applied to the preliminary design of two wings for the flying unmanned aerial vehicle demonstrator developed within the FLEXOP project. Two wing designs, the reference wing employing symmetric-balanced laminates and the tailored wing employing symmetric-unbalanced laminates, were developed. A significant reduction in structural mass of 4% was observed in the tailored wing which, in the end, translates to a 1% reduction in mass at the aircraft level. In addition to mass savings, a reduction in root loads was observed. The bending moment was reduced by 6% and 11% in the $5g$ and $-2g$ load cases, respectively, relative the reference wing.

It should be noted that the design requirements imposed by the FLEXOP project had a strong influence on the results obtained. The structural layout of the wings in terms of rib and spar positions was not subject to optimization and led to a design which was predominantly driven by the buckling constraint in the wing skins and the minimum thickness constraint in the spars. To further improve the designs, the structural layout of the wing should also be included in the optimization. In this way, the strength of the composite material and aeroelastic properties of the wing can be further exploited to achieve additional mass savings and load reductions.

For production reasons, the material reference axis was fixed along the rear spar of the wing for all the laminate design regions, thereby driving the tailoring of the reference wing by defining the axis with respect to which the laminate is balanced. In case of the tailored wing, the use of unbalanced laminates means its design is not affected by the choice of the material reference axis. Hence, it is possible that the reference wing could be further improved if the material reference axis could have been freely chosen and thus included in the optimization as a design variable.

The introduction of the wing jig and cruise shape as a design variable and constraint, respectively, in the optimization have been successfully demonstrated. This resulted in a nearly identical aeroelastic response in terms of lift distribution and local angle of attack between both wings in the $1g$ load case. However, to achieve this, the reference wing requires significantly more pretwist in its jig shape than the tailored wing. At the wing tip, the reference wing required a pretwist of -1.38 deg, while the tailored wing only required a pretwist of -0.59 deg, which, consequently, had an adverse effect on the maneuver load alleviation capability of the reference wing in the negative load cases.

In the current design study, the cruise shape constraint was enforced using a single load case. The presented approach where the jig shape is an integral part of the optimization process, however, allows for the integration of a cruise shape constraint or tradeoff across multiple load cases. In this way, design studies in which the cruise condition consists of a range of load cases, due to the changing aircraft mass and flight altitude, can be facilitated. Especially for aeroelastically tailored wings, which tend to be tailored for a specific set of load cases during their design, applying the cruise shape constraint across several cruise load cases could have an important effect on the retrieved jig shape and on the maneuver load alleviation capabilities of the derived wing designs.

From the optimization point of view, the use of lamination parameters and thickness to parameterize the laminates yields the best possible designs. In practice, however, the stacking sequence retrieval required to obtain manufacturable laminates cannot completely match the optimized lamination parameters and thicknesses; hence some loss in maneuver load alleviation and increase in structural weight are to be expected.

To summarize, the current design study highlights the capabilities and benefits of aeroelastic composite tailoring for maneuver load alleviation and corresponding reduction of the structural mass of aircraft wings by presenting two wing designs for a flying demonstrator. In the future, this assessment could be further improved by extending the design space to include the structural layout and the material reference axis of the wing, by allowing the cruise shape constraint to cover several cruise load cases, and by including the effect of the stacking sequence retrieval from the lamination parameters, preferably by including additional constraints on the lamination parameters in the optimization.

Appendix A: Design Requirements and Constraints

Table A1 FLEXOP design requirements

Parameter	Value
Wing planform	
Span, m	3.536
Chord root/tip chord, m	0.471/0.236
Leading edge sweep, deg	20
Airfoil	try6
Airfoil thickness root/tip, %	10/8 chord
Structural layout	
Front/rear spar position, % chord	15/71
Rib spacing	See Table A3
Leading/trailing edge	Exclude from optimization
Material properties	
Material	C 8552S/34%/UD134/AS4
Laminate reference axis	Along the rear spar
Knockdown factors	90oC/W/BVID
Control surface layout	
Number of flaps	1
Spanwise start/end, %	12/33 span
Chordwise start/end, %	75/100 chord
Deflection range up/down, deg	5/60
Number of ailerons	3
Spanwise start/end, %	33/55/77/98 span
Chordwise start/end, % chord	75/100 (all)
Deflection up/down, deg	25/25
Operating conditions	
Atmosphere type	International standard atmosphere (ISA)
Cruise/landing indicated airspeed (IAS), m/s	45/20
Cruise/landing altitude, m	800/500
Max. positive load	$5g$ at cruise speed and altitude
Max. negative load	$-2g$ at cruise speed and altitude
Load safety factor (LSF)	1.5
Design problem	
Objective	Mass minimization
Design variables	Thickness + stiffness
Spanwise design regions	11 (+1)
Chordwise design regions	1

Table A2 FLEXOP design constraints

Parameter	Value
Laminate constraints	
Lamination parameters	Feasibility constraints (see Hammer et al. [48], Raju et al. [49] and Wu et al. [50])
Thickness min./max., mm	1.0/12.5
Strength and buckling constraints	
Strength properties	$<1/\text{LSF} * \text{KDF} * \text{material allowables}$
Buckling multiplier	$<1/\text{LSF} * \text{KDF}$
Aeroelastic constraints	
Control effectiveness	>0.15
Flutter/divergence	$\text{Re}(\lambda_i) < 0$
Cruise shape constraint	
Twist distribution	Linear
Twist at root/tip, deg	0/−2
Twist tolerance, deg	±0.05

Table A3 Spanwise rib distribution

Rib number	Span, m	Orientation
1	0.108	FD[a]
2	0.150	FD
3	0.284	FD
4	0.423	FD
5	0.491	RS[b]
6	0.596	RS
7	0.696	RS
8	0.761	RS
9	0.897	RS
10	1.036	RS
11	1.178	RS
12	1.314	RS
13	1.379	RS
14	1.528	RS
15	1.681	RS
16	1.835	RS
17	1.992	RS
18	2.152	RS
19	2.216	RS
20	2.388	RS
21	2.572	RS
22	2.760	RS
23	2.825	RS
24	3.022	RS
25	3.233	RS
26	3.466	FD
27	3.535	FD

[a]FD means in the direction of flight.
[b]RS means normal to the rear spar.

Appendix B: Wing Design Parameters

Table B1 Values of design variables for the reference wing (V2A, V4A, V2D, and V4D = 0 for all structural members in all design regions)

DV[a]	DR[b] 1	DR 2	DR 3	DR 4	DR 5	DR 6	DR 7	DR 8	DR 9	DR 10	DR 11	DR 12
Top skin												
V1A	−0.141	−0.118	−0.114	−0.128	−0.143	−0.194	−0.314	−0.372	−0.467	−0.344	−0.528	−0.218
V3A	−0.039	−0.106	−0.087	−0.088	−0.133	−0.160	−0.176	−0.249	−0.278	−0.172	−0.260	−0.114
V1D	0.466	0.471	0.482	0.465	0.431	0.359	0.187	0.063	−0.130	−0.307	−0.257	0.006
V3D	−0.566	−0.556	−0.355	−0.328	−0.628	−0.742	−0.687	−0.822	−0.777	−0.572	−0.638	−0.571
t, mm	3.48	3.87	3.30	3.19	3.52	3.35	3.10	2.96	2.64	2.25	1.93	1.39
Bottom skin												
V1A	0.034	0.034	−0.014	−0.015	−0.069	−0.099	−0.097	−0.169	−0.173	−0.098	−0.117	−0.012
V3A	0.031	0.016	−0.009	−0.009	−0.041	−0.056	−0.053	−0.092	−0.097	−0.060	−0.075	−0.018
V1D	0.408	0.488	0.415	0.377	0.523	0.472	0.155	0.160	−0.037	−0.290	−0.267	−0.007

Table B1 (*Continued.*)

DV[a]	DR[b] 1	DR 2	DR 3	DR 4	DR 5	DR 6	DR 7	DR 8	DR 9	DR 10	DR 11	DR 12
V3D	−0.666	−0.523	−0.331	−0.311	−0.453	−0.543	−0.493	−0.574	−0.656	−0.493	−0.547	−0.489
t, mm	2.60	2.84	2.45	2.39	2.59	2.48	2.37	2.26	2.04	1.71	1.53	1.05
						Front spar						
V1A	0.056	0.092	0.056	0.051	0.108	0.104	0.073	0.088	0.073	0.049	0.071	0.079
V3A	0.041	0.040	0.020	0.019	0.030	0.026	0.016	0.009	0.002	0.000	0.003	0.018
V1D	−0.094	−0.094	−0.094	−0.094	−0.094	−0.095	−0.094	−0.094	−0.094	−0.094	−0.094	−0.094
V3D	−0.750	−0.750	−0.750	−0.750	−0.750	−0.750	−0.750	−0.750	−0.750	−0.750	−0.750	−0.750
T, mm	1.02	1.02	1.02	1.02	1.02	1.02	1.02	1.02	1.02	1.02	1.02	1.02
						Rear spar						
V1A	0.012	0.019	0.011	0.009	0.017	0.015	0.011	0.016	0.015	0.005	0.012	0.009
V3A	0.011	0.015	0.011	0.009	0.017	0.017	0.013	0.020	0.020	0.011	0.016	0.008
V1D	−0.094	−0.094	−0.094	−0.094	−0.094	−0.094	−0.094	−0.094	−0.094	−0.094	−0.094	−0.094
V3D	−0.750	−0.750	−0.750	−0.750	−0.750	−0.750	−0.750	−0.750	−0.750	−0.750	−0.750	−0.750
t, mm	1.02	1.02	1.02	1.02	1.02	1.02	1.02	1.02	1.02	1.02	1.02	1.02

[a]DV means design variable.
[b]DR means design region.

Table B2 Values of design variables for the reference wing

DV	DR[a] 1	DR 2	DR 3	DR 4	DR 5	DR 6	DR 7	DR 8	DR 9	DR 10	DR 11	DR 12
						Top skin						
V1A	−0.093	−0.092	−0.103	−0.113	−0.162	−0.238	−0.330	−0.352	−0.393	−0.483	−0.444	−0.311
V2A	0.015	0.005	−0.079	−0.090	−0.179	−0.254	−0.267	−0.372	−0.360	−0.288	−0.267	0.008
V3A	−0.037	−0.114	−0.091	−0.087	−0.161	−0.188	−0.184	−0.274	−0.267	−0.224	−0.275	−0.154
V4A	0.017	0.006	−0.074	−0.084	−0.190	−0.273	−0.265	−0.429	−0.370	−0.263	−0.273	0.008
V1D	0.516	0.498	0.489	0.478	0.351	0.191	0.039	−0.267	−0.323	−0.386	−0.264	0.005
V2D	−0.072	0.025	−0.059	−0.073	−0.075	−0.143	−0.167	−0.327	−0.285	−0.177	−0.179	−0.036
V3D	−0.464	−0.433	−0.266	−0.253	−0.610	−0.745	−0.750	−0.779	−0.715	−0.560	−0.680	−0.626
V4D	0.001	0.343	0.510	0.531	0.426	0.502	0.633	0.525	0.526	0.599	0.635	0.646
t, mm	3.37	3.79	3.21	3.10	3.45	3.28	3.02	2.96	2.63	2.09	1.86	1.30
						Bottom skin						
V1A	0.054	0.059	−0.029	−0.034	−0.124	−0.176	−0.259	−0.322	−0.375	−0.251	−0.306	0.041
V2A	−0.042	−0.036	0.054	0.071	0.192	0.271	0.279	0.415	0.391	0.219	0.204	−0.030
V3A	0.042	0.029	−0.015	−0.015	−0.044	−0.059	−0.078	−0.125	−0.157	−0.098	−0.152	0.003
V4A	−0.039	−0.034	0.051	0.066	0.176	0.250	0.243	0.447	0.399	0.194	0.184	−0.028
V1D	0.466	0.493	0.452	0.436	0.428	0.311	0.189	−0.189	−0.284	−0.304	−0.260	0.008
V2D	0.135	0.007	0.096	0.109	0.057	0.126	0.153	0.379	0.327	0.160	0.166	0.206
V3D	−0.556	−0.395	−0.269	−0.261	−0.456	−0.562	−0.584	−0.769	−0.709	−0.533	−0.592	−0.434
V4D	0.001	−0.401	−0.548	−0.571	−0.460	−0.533	−0.658	−0.629	−0.626	−0.673	−0.662	−0.680
t, mm	2.47	2.73	2.32	2.24	2.48	2.37	2.18	2.10	1.85	1.58	1.37	1.02
						Front spar						
V1A	0.065	0.115	0.071	0.063	0.128	0.121	0.085	0.119	0.103	0.055	0.084	0.072
V2A	−0.010	−0.046	−0.027	−0.027	−0.048	−0.049	−0.039	−0.054	−0.051	−0.038	−0.052	−0.023
V3A	0.042	0.050	0.024	0.022	0.038	0.030	0.018	0.022	0.015	0.002	0.009	0.021
V4A	−0.009	−0.044	−0.026	−0.025	−0.047	−0.048	−0.038	−0.054	−0.050	−0.037	−0.051	−0.022
V1D	−0.094	−0.095	−0.094	−0.094	−0.095	−0.094	−0.094	−0.094	−0.094	−0.094	−0.094	−0.094
V2D	−0.281	−0.281	−0.281	−0.281	−0.281	−0.281	−0.281	−0.281	−0.281	−0.281	−0.281	−0.281
V3D	−0.750	−0.750	−0.750	−0.750	−0.750	−0.750	−0.750	−0.750	−0.750	−0.750	−0.750	−0.750
V4D	0.000	0.000	0.000	0.000	0.000	0.000	0.000	0.000	0.000	0.000	0.000	0.000
t, mm	1.02	1.02	1.02	1.02	1.02	1.02	1.02	1.02	1.02	1.02	1.02	1.02
						Rear spar						
V1A	0.014	0.025	0.013	0.012	0.020	0.018	0.014	0.019	0.015	0.012	0.024	0.010
V2A	0.014	0.007	0.006	0.005	0.012	0.012	0.009	0.014	0.013	0.006	0.007	0.006
V3A	0.012	0.017	0.012	0.010	0.020	0.020	0.015	0.023	0.021	0.015	0.023	0.009
V4A	0.013	0.007	0.006	0.005	0.011	0.011	0.008	0.013	0.012	0.005	0.006	0.006
V1D	−0.094	−0.094	−0.094	−0.094	−0.094	−0.094	−0.094	−0.094	−0.094	−0.094	−0.094	−0.094
V2D	−0.281	−0.281	−0.281	−0.281	−0.281	−0.281	−0.281	−0.281	−0.281	−0.281	−0.281	−0.281
V3D	−0.750	−0.750	−0.750	−0.750	−0.750	−0.750	−0.750	−0.750	−0.750	−0.750	−0.750	−0.750
V4D	0.000	0.000	0.000	0.000	0.000	0.000	0.000	0.000	0.000	0.000	0.000	0.000
t, mm	1.02	1.02	1.02	1.02	1.02	1.02	1.02	1.02	1.02	1.02	1.02	1.02

[a]DR means design region.

Acknowledgments

The work presented herein has been partially funded by the European Community's Horizon 2020 Programme under the grant agreement 636307. The Flutter Free Flight Envelope Expansion for Economical Performance Improvement is a project funded under the topic MG-1.1-2014, involving ten partners. The project started on 1 June 2015.

References

[1] Haftka, R. T., "Optimization of Flexible Wing Structures Subject to Strength and Induced Drag Constraints," *AIAA Journal*, Vol. 15, No. 8, 1977, pp. 1101–1106. https://doi.org/10.2514/3.7400

[2] Grossman, B., Gurdal, Z., Strauch, G. J., Eppard, W. M., and Haftka, R. T., "Integrated Aerodynamic/Structural Design of a Sailplane Wing," *Journal of Aircraft*, Vol. 25, No. 9, 1988, pp. 855–860. https://doi.org/10.2514/3.45670

[3] Stodieck, O., Cooper, J. E., Weaver, P. M., and Kealy, P., "Aeroelastic Tailoring of a Representative Wing Box Using Tow-Steered Composites," *AIAA Journal*, Vol. 55, No. 4, 2017, pp. 1425–1439. https://doi.org/10.2514/1.J055364

[4] Kenway, G. K. W., and Martins, J. R. R. A., "Multipoint High-Fidelity Aerostructural Optimization of a Transport Aircraft Configuration," *Journal of Aircraft*, Vol. 51, No. 1, 2014, pp. 144–160. https://doi.org/10.2514/1.C032150

[5] Brooks, T. R., Martins, J. R., and Kennedy, G. J., "High-Fidelity Aerostructural Optimization of Tow-Steered Composite Wings," *Journal of Fluids and Structures*, Vol. 88, July 2019, pp. 122–147. https://doi.org/10.1016/j.jfluidstructs.2019.04.005

[6] Achard, T., Blondeau, C., and Ohayon, R., "High-Fidelity Aerostructural Gradient Computation Techniques with Application to a Realistic Wing Sizing," *AIAA Journal*, Vol. 56, No. 11, 2018, pp. 4487–4499. https://doi.org/10.2514/1.J056736

[7] Aly, S., Ogot, M., Pelz, R., and Siclari, M., "Jig-Shape Static Aeroelastic Wing Design Problem: A Decoupled Approach," *Journal of Aircraft*, Vol. 39, No. 6, 2002, pp. 1061–1066. https://doi.org/10.2514/2.3035

[8] Stanford, B. K., Jutte, C. V., and Wieseman, C. D., "Trim and Structural Optimization of Subsonic Transport Wings Using Nonconventional Aeroelastic Tailoring," *AIAA Journal*, Vol. 54, No. 1, 2016, pp. 293–309. https://doi.org/10.2514/1.J054244

[9] Livne, E., Schmit, L. A., and Friedmann, P. P., "Integrated Structure/Control/Aerodynamic Synthesis of Actively Controlled Composite Wings," *Journal of Aircraft*, Vol. 30, No. 3, 1993, pp. 387–394. https://doi.org/10.2514/3.46347

[10] Livne, E., "Integrated Aeroservoelastic Optimization: Status and Direction," *Journal of Aircraft*, Vol. 36, No. 1, 1999, pp. 122–145. https://doi.org/10.2514/2.2419

[11] Kenway, G., Kennedy, G., and Martins, J., "A CAD-Free Approach to High-Fidelity Aerostructural Optimization," *13th AIAA/ISSMO Multidisciplinary Analysis Optimization Conference*, AIAA Paper 2010-9231, 2010. https://doi.org/10.2514/6.2010-9231

[12] Stanford, B. K., and Dunning, P. D., "Optimal Topology of Aircraft Rib and Spar Structures Under Aeroelastic Loads," *Journal of Aircraft*, Vol. 52, No. 4, 2015, pp. 1298–1311. https://doi.org/10.2514/1.C032913

[13] Stanford, B. K., "Aeroelastic Wingbox Stiffener Topology Optimization," *Journal of Aircraft*, Vol. 55, No. 3, 2018, pp. 1244–1251. https://doi.org/10.2514/1.C034653

[14] De, S., Jrad, M., and Kapania, R. K., "Structural Optimization of Internal Structure of Aircraft Wings with Curvilinear Spars and Ribs," *Journal of Aircraft*, Vol. 56, No. 2, 2019, pp. 707–718. https://doi.org/10.2514/1.C034818

[15] Zhao, W., and Kapania, R. K., "Bilevel Programming Weight Minimization of Composite Flying-Wing Aircraft with Curvilinear Spars and Ribs," *AIAA Journal*, Vol. 57, No. 6, 2019, pp. 2594–2608. https://doi.org/10.2514/1.J057892

[16] Shirk, M. H., Hertz, T. J., and Weisshaar, T. A., "Aeroelastic Tailoring–Theory, Practice, and Promise," *Journal of Aircraft*, Vol. 23, No. 1, 1986, pp. 6–18. https://doi.org/10.2514/3.45260

[17] Qin, Z., Marzocca, P., and Librescu, L., "Aeroelastic Instability and Response of Advanced Aircraft Wings at Subsonic Flight Speeds," *Aerospace Science and Technology*, Vol. 6, No. 3, 2002, pp. 195–208. https://doi.org/10.1016/S1270-9638(02)01158-6

[18] Qin, Z., Librescu, L., and Marzocca, P., "Aeroelasticity of Composite Aerovehicle Wings in Supersonic Flows," *Journal of spacecraft and rockets*, Vol. 40, No. 2, 2003, pp. 162–173. https://doi.org/10.2514/2.3950

[19] Weisshaar, T. A., "Aeroelastic Tailoring–Creative Uses of Unusual Materials,"*28th Structures, Structural Dynamics and Materials Conference*, AIAA Paper 1987-976, 1987. https://doi.org/10.2514/6.1987-976

[20] Danilin, A., and Weisshaar, T. A., "The Use of Optimality Criteria for Aircraft Conceptual Level Structural Design," *41st AIAA/ASME/ASCE/AHS Structural Dynamics and Materials Conference*, AIAA Paper 2000-1328, 2000.

[21] Livne, E., and Weisshaar, T. A., "Aeroelasticity of Nonconventional Airplane Configurations—Past and Future," *Journal of Aircraft*, Vol. 40, No. 6, 2003, pp. 1047–1065. https://doi.org/10.2514/2.7217

[22] Weisshaar, T. A., and Duke, D. K., "Induced Drag Reduction Using Aeroelastic Tailoring with Adaptive Control Surfaces," *Journal of Aircraft*, Vol. 43, No. 1, 2006, pp. 157–164. https://doi.org/10.2514/1.12040

[23] Eastep, F. E., Tischler, V. A., Venkayya, V. B., and Khot, N. S., "Aeroelastic Tailoring of Composite Structures," *Journal of Aircraft*, Vol. 36, No. 6, 1999, pp. 1041–1047. https://doi.org/10.2514/2.2546

[24] Arizono, H., and Isogai, K., "Application of Genetic Algorithm for Aeroelastic Tailoring of a Cranked-Arrow Wing," *Journal of Aircraft*, Vol. 42, No. 2, 2005, pp. 493–499. https://doi.org/10.2514/1.392

[25] Guo, S. J., Bannerjee, J. R., and Cheung, C. W., "The Effect of Laminate Lay-Up on the Flutter Speed of Composite Wings," *Journal of Aerospace Engineering*, Vol. 217, No. 3, 2003, pp. 115–122. https://doi.org/10.1243/095441003322297225

[26] Guo, S., Cheng, W., and Cui, D., "Optimization of Composite Wing Structures for Maximum Flutter Speed," *46th AIAA/ASME/ASCE/AHS/ASC Structures, Structural Dynamics and Materials Conference*, AIAA Paper 2005-2132, 2005. https://doi.org/10.2514/6.2005-2132

[27] Dillinger, J. K. S., Abdalla, M. M., Klimmek, T., and Gürdal, Z., "Static Aeroelastic Stiffness Optimization and Investigation of Forward Swept Composite Wings," *10th World Congress on Structural and Multidisciplinary Optimization*, ufl.edu, Orlando, FL, 2013, pp. 1–10.

[28] Dillinger, J. K. S., Abdalla, M. M., Meddaikar, Y. M., and Klimmek, T., "Static Aeroelastic Stiffness Optimization of a Forward Swept Composite Wing with CFD-Corrected Aero Loads," *CEAS Aeronautical Journal*, Vol. 10, No. 4, 2019, pp. 1015–1032. https://doi.org/10.1007/s13272-019-00397-y

[29] Guo, S. J., Cheng, W., and Cui, D., "Aeroelastic Tailoring of Composite Wing Structures by Laminate Layup Optimization," *AIAA Journal*, Vol. 44, No. 12, 2006, pp. 3146–3150. https://doi.org/10.2514/1.20166

[30] Kameyama, M., and Fukunaga, H., "Optimum Design of Composite Plate Wings for Aeroelastic Characteristics Using Lamination Parameters," *Computers and Structures*, Vol. 85, Nos. 3–4, 2007, pp. 213–224. https://doi.org/10.1016/j.compstruc.2006.08.051

[31] Manan, A., Vio, G. A., Harmin, M. Y., and Cooper, J. E., "Optimization of Aeroelastic Composite Structures Using Evolutionary Algorithms," *Engineering Optimization*, Vol. 42, No. 2, 2010, pp. 171–184. https://doi.org/10.1080/03052150903104358

[32] De Leon, D. M., De Souza, C. E., Fonseca, J. S. O., and Da Silva, R. G. A., "Aeroelastic Tailoring Using Fiber Orientation and Topology Optimization," *Structural and Multidisciplinary Optimization*, Vol. 46, No. 5, 2012, pp. 663–677. https://doi.org/10.1007/s00158-012-0790-8

[33] Pettit, C. L., and Grandhi, R. V., "Optimization of a Wing Structure for Gust Response and Aileron Effectiveness," *Journal of Aircraft*, Vol. 40, No. 6, 2003, pp. 1185–1191.

[34] Kim, T. U., and Hwang, I. H., "Optimal Design of Composite Wing Subjected to Gust Loads," *Computers and Structures*, Vol. 83, Nos. 19–20, 2005, pp. 1546–1554. https://doi.org/10.1016/j.compstruc.2005.02.002

[35] Thuwis, G. A. A., De Breuker, R., Abdalla, M. M., and Gürdal, Z., "Aeroelastic Tailoring Using Lamination Parameters: Drag Reduction of a Formula One Rear Wing," *Structural and Multidisciplinary Optimization*, Vol. 41, No. 4, 2010, pp. 637–646. https://doi.org/10.1007/s00158-009-0437-6

[36] Sherrer, V. C., Hertz, T. J., and Shirk, M. H., "Wind Tunnel Demonstration of Aeroelastic Tailoring Applied to Forward Swept Wings," *Journal of Aircraft*, Vol. 18, No. 11, 1981, pp. 976–983. https://doi.org/10.2514/3.57589

[37] Blair, M., and Weisshaar, T. A., "Swept Composite Wing Aeroelastic Divergence Experiments," *Journal of Aircraft*, Vol. 19, No. 11, 1982, pp. 1019–1024. https://doi.org/10.2514/3.44806

[38] Hollowell, S. J., and Dugundji, J., "Aeroelastic Flutter and Divergence of Stiffness Coupled, Graphite/Epoxy Cantilevered Plates," *Journal of Aircraft*, Vol. 21, No. 1, 1984, pp. 69–76. https://doi.org/10.2514/3.48224

[39] Landsberger, B. J., and Dugundji, J., "Experimental Aeroelastic Behavior of Unswept and Forward-Swept Cantilever Graphite/Epoxy Wings," *Journal of Aircraft*, Vol. 22, No. 8, 1985, pp. 679–686. https://doi.org/10.2514/3.45186

[40] Chen, G.-S., and Dugundji, J., "Experimental Aeroelastic Behavior of Forward-Swept Graphite/Epoxy Wings with Rigid-Body Freedom," *Journal of Aircraft*, Vol. 24, No. 7, 1987, pp. 454–462. https://doi.org/10.2514/3.45501

[41] Werter, N. P. M., Sodja, J., and De Breuker, R., "Design and Testing of Aeroelastically Tailored Wings Under Maneuver Loading," *AIAA Journal*, Vol. 55, No. 3, 2017, pp. 1012–1025. https://doi.org/10.2514/1.J054965

[42] Sodja, J., Werter, N. P. M., Dillinger, J. K. S., and De Breuker, R., "Dynamic Response of Aeroelastically Tailored Composite Wing: Analysis and Experiment," *57th AIAA/ASCE/AHS/ASC Structures, Structural Dynamics, and Materials Conference*, AIAA Paper 2016-0469, 2016. https://doi.org/10.2514/6.2016-0469

[43] Werter, N. P. M., and De Breuker, R., "A novel Dynamic Aeroelastic Framework for Aeroelastic Tailoring and Structural Optimisation," *Composite Structures*, Vol. 158, Dec. 2016, pp. 369–386. https://doi.org/10.1016/j.compstruct.2016.09.044

[44] Werter, N., "Aeroelastic Modelling and Design of Aeroelastically Tailored and Morphing Wings," Ph.D. Dissertation, Delft Univ. of Technology, Delft, The Netherlands, 2017. https://doi.org/10.4233/UUID:74925F40-1EFC-469F-88EE-E871C720047E

[45] Ferede, E., and Abdalla, M., "Cross-Sectional Modelling of Thin-Walled Composite Beams," *55th AIAA/ASME/ASCE/AHS/ASC Structures, Structural Dynamics, and Materials Conference*, AIAA Paper 2014-0163, 2014. https://doi.org/10.2514/6.2014-0163

[46] IJsselmuiden, S. T., Abdalla, M. M., and Gürdal, Z., "Implementation of Strength-Based Failure Criteria in the Lamination Parameter Design Space," *AIAA Journal*, Vol. 46, No. 7, 2008, pp. 1826–1834. https://doi.org/10.2514/1.35565

[47] Khani, A., IJsselmuiden, S., Abdalla, M., and Gürdal, Z., "Design of Variable Stiffness Panels for Maximum Strength Using Lamination Parameters," *Composites Part B: Engineering*, Vol. 42, No. 3, 2011, pp. 546–552. https://doi.org/10.1016/j.compositesb.2010.11.005

[48] Hammer, V., Bendsøe, M., Lipton, R., and Pedersen, P., "Parametrization in Laminate Design for Optimal Compliance," *International Journal of Solids and Structures*, Vol. 34, No. 4, 1997, pp. 415–434. https://doi.org/10.1016/S0020-7683(96)00023-6

[49] Raju, G., Wu, Z., and Weaver, P., "On Further Developments of Feasible Region of Lamination Parameters for Symmetric Composite Laminates," *55th AIAA/ASME/ASCE/AHS/ASC Structures, Structural Dynamics, and Materials Conference*, AIAA Paper 2014-1374, 2014. https://doi.org/10.2514/6.2014-1374

[50] Wu, Z., Raju, G., and Weaver, P. M., "Framework for the Buckling Optimization of Variable-Angle Tow Composite Plates," *AIAA Journal*, Vol. 53, No. 12, 2015, pp. 3788–3804. https://doi.org/10.2514/1.J054029

[51] De Breuker, R., Abdalla, M. M., and Gürdal, Z., "Design of Morphing Winglets with the Inclusion of Nonlinear Aeroelastic Effects," *Aeronautical Journal*, Vol. 115, No. 1174, 2011, pp. 713–728.

[52] Werter, N., De Breuker, R., Friswell, M., Dettmer, W., and Beaverstock, C. S., "Two-Level Conceptual Design of Morphing Wings," *54th AIAA/ASME/ASCE/AHS/ASC Structures, Structural Dynamics, and Materials Conference*, AIAA Paper 2013-1720, 2013. https://doi.org/10.2514/6.2013-1720

[53] Kassapoglou, C., *Design and Analysis of Composite Structures*, Wiley, Hoboken, NJ, 2013, pp. 65–152. https://doi.org/10.1002/9781118536933

[54] Dillinger, J., "Static Aeroelastic Optimization of Composite Wings with Variable Stiffness Laminates," Ph.D. Dissertation, Delft Univ. of Technology, Delft, The Netherlands, 2014. https://doi.org/10.4233/uuid:20484651-fd5d-49f2-9c56-355bc680f2b7